Journal Pre-proof

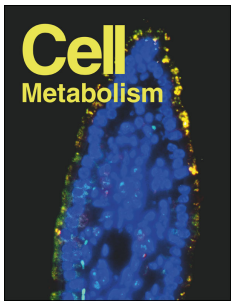

Expression of SARS-CoV-2 Entry Factors in the Pancreas of Normal Organ Donors and Individuals with COVID-19

Irina Kusmartseva, Wenting Wu, Farooq Syed, Verena Van Der Heide, Marda Jorgensen, Paul Joseph, Xiaohan Tang, Eduardo Candelario-Jalil, Changjun Yang, Harry Nick, Jack L. Harbert, Amanda L. Posgai, John David Paulsen, Richard Lloyd, Sirlene Cechin, Alberto Pugliese, Martha Campbell-Thompson, Richard S. Vander Heide, Carmella Evans-Molina, Dirk Homann, Mark A. Atkinson

PII: S1550-4131(20)30600-8

DOI: https://doi.org/10.1016/j.cmet.2020.11.005

Reference: CMET 3142

To appear in: *Cell Metabolism*

Received Date: 1 September 2020

Revised Date: 19 October 2020

Accepted Date: 10 November 2020

Please cite this article as: Kusmartseva, I., Wu, W., Syed, F., Van Der Heide, V., Jorgensen, M., Joseph, P., Tang, X., Candelario-Jalil, E., Yang, C., Nick, H., Harbert, J.L., Posgai, A.L., Paulsen, J.D., Lloyd, R., Cechin, S., Pugliese, A., Campbell-Thompson, M., Vander Heide, R.S., Evans-Molina, C., Homann, D., Atkinson, M.A., Expression of SARS-CoV-2 Entry Factors in the Pancreas of Normal Organ Donors and Individuals with COVID-19 *Cell Metabolism* (2020), doi: https://doi.org/10.1016/j.cmet.2020.11.005.

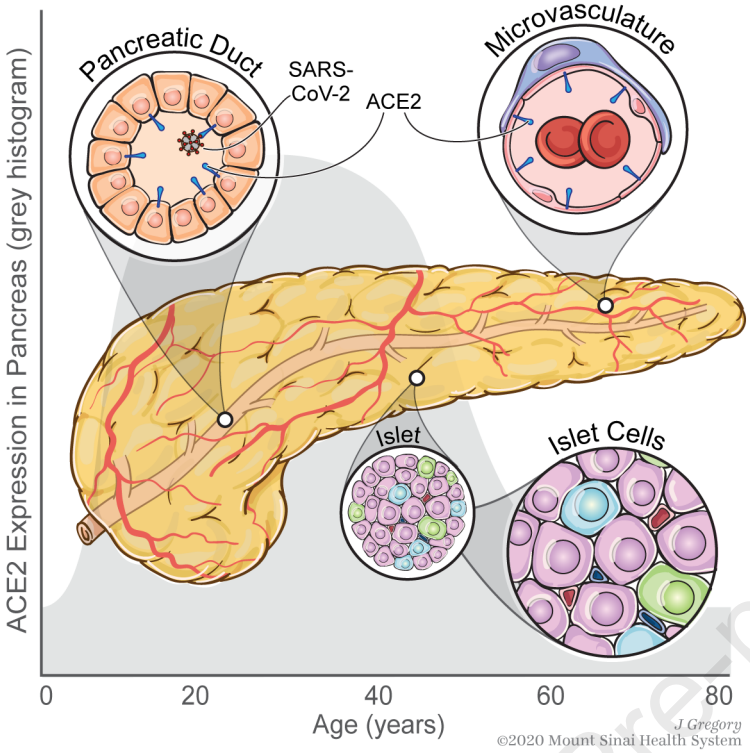

Short Article

Expression of SARS-CoV-2 Entry Factors in the Pancreas of Normal Organ Donors and Individuals with COVID-19

Irina Kusmartseva[1*], Wenting Wu[2,3,4*], Farooq Syed[2,3*], Verena Van Der Heide[5*], Marda Jorgensen[1*], Paul Joseph[1], Xiaohan Tang[1,6], Eduardo Candelario-Jalil[7], Changjun Yang[7], Harry Nick[7], Jack L. Harbert[8], Amanda L. Posgai[1], John David Paulsen[9], Richard Lloyd[10], Sirlene Cechin[11], Alberto Pugliese[11], Martha Campbell-Thompson[1,12], Richard S. Vander Heide[8], Carmella Evans-Molina[2,3,13], Dirk Homann[5], Mark A. Atkinson[1,14†]

[1]Department of Pathology, Immunology, and Laboratory Medicine, University of Florida Diabetes Institute, College of Medicine, Gainesville, Florida 32610, USA
[2]Center for Diabetes and Metabolic Diseases, Indiana University School of Medicine, Indianapolis, Indiana 46202, USA
[3]Herman B. Wells Center for Pediatric Research, Indiana University School of Medicine, Indianapolis, Indiana 46202, USA
[4]Department of Medical and Molecular Genetics, Indiana University School of Medicine, Indianapolis, Indiana 46202, USA
[5]Department of Medicine, Diabetes Obesity & Metabolism Institute and Precision Immunology Institute, Icahn School of Medicine at Mount Sinai, New York, New York 10029 USA
[6]Department of Metabolism and Endocrinology, The Second Xiangya Hospital, Central South University, Changsha, Hunan 410011, China
[7]Department of Neuroscience, College of Medicine, Gainesville, Florida 32610, USA
[8]Department of Pathology, Louisiana State University, New Orleans, Louisiana 70112, USA
[9]Department of Pathology, Molecular and Cell-Based Medicine, Icahn School of Medicine at Mount Sinai, New York, 10029 New York USA
[10]Department of Virology and Microbiology, Baylor College of Medicine, Houston, Texas 77030, USA
[11]Diabetes Research Institute, Department of Medicine, Division of Endocrinology, Diabetes and Metabolism, Department of Microbiology and Immunology, Miller School of Medicine, University of Miami, Miami, Florida, USA
[12]Department of Biomedical Engineering, University of Florida, College of Engineering, Gainesville, Florida 32610, USA
[13]Roudebush VA Medical Center, Indianapolis, Indiana 46202, USA
[14]Department of Pediatrics, University of Florida Diabetes Institute, College of Medicine, Gainesville, Florida 32610, USA
*These authors contributed equally

Correspondence: atkinson@ufl.edu

Characters: 35,126; Abstract 150; Figures 5; Supplemental Figures 5; Supplemental Tables 4

† Lead Contact

SUMMARY

Diabetes is associated with increased mortality from Severe Acute Respiratory Syndrome Coronavirus-2 (SARS-CoV-2). Given literature suggesting a potential association between SARS-CoV-2 infection and diabetes induction, we examined pancreatic expression of angiotensin-converting enzyme-2 (ACE2), the key entry factor for SARS-CoV-2 infection. Specifically, we analyzed five public scRNA-seq pancreas datasets and performed fluorescence *in situ* hybridization, Western blotting and immunolocalization for ACE2 with extensive reagent validation on normal human pancreatic tissues across the lifespan, as well as those from coronavirus disease 2019 (COVID-19) cases. These *in silico* and *ex vivo* analyses demonstrated prominent expression of ACE2 in pancreatic ductal epithelium and microvasculature, but we found rare endocrine cell expression at the mRNA-level. Pancreata from individuals with COVID-19 demonstrated multiple thrombotic lesions with SARS-CoV-2 nucleocapsid protein expression that was primarily limited to ducts. These results suggest SARS-CoV-2 infection of pancreatic endocrine cells, via ACE2, is an unlikely central pathogenic feature of COVID-19-related diabetes.

KEYWORDS: SARS-CoV-2, COVID-19, type 1 diabetes, type 2 diabetes, pancreas, ACE2, TMPRSS2, islet, CD34, insulin

INTRODUCTION

The coronavirus disease 2019 (COVID-19) pandemic caused by Severe Acute Respiratory Syndrome-Coronavirus-2 (SARS-CoV-2) has created a global healthcare crisis (Mercatelli and Giorgi, 2020). With infections continuing to rise in many countries and the potential for continuing viral persistence in the absence of a vaccine, there is an urgent need to better understand SARS-CoV-2-mediated pathology. Key to this are efforts examining human tissues potentially susceptible to infection.

While initial reports primarily focused on pulmonary and cardiovascular manifestations, other organs including the kidney, brain and intestines, as well as the pancreas, have since been noted as affected by this disorder's pathophysiology (Connors and Levy, 2020; Fox et al., 2020; Hanley et al., 2020; Lee et al., 2020b; Liu et al., 2020; Menter et al., 2020; Rapkiewicz et al., 2020; Varga et al., 2020; Wang et al., 2020; Wichmann et al., 2020). Indeed, recent reports have raised the question of whether SARS-CoV-2 might infect the pancreas and possibly potentiate or exacerbate diabetes in either of its predominant forms, type 1 or type 2 diabetes (i.e., T1D or T2D, respectively). These studies noted elevated serum levels of the exocrine pancreatic enzymes, amylase and lipase, as well as development or worsening of hyperglycemia in SARS-CoV-2-positive individuals (Wang et al., 2020), high prevalence of diabetic ketoacidosis in people hospitalized with COVID-19 (Goldman et al., 2020; Li et al., 2020), and increased COVID-19-induced mortality in those with T1D and T2D (Barron et al., 2020; Holman et al., 2020). Reports also include increased incidence of new-onset T1D in specific geographic clusters (Unsworth et al., 2020), case reports linking the timing of T1D onset to COVID-19 (Marchand et al., 2020), and pancreatic expression of angiotensin-converting enzyme-2 (ACE2) through which SARS-CoV-2 could gain access to cells (Chen and Hao, 2020), potentially including in insulin-producing β-cells (Lee et al., 2020b; Yang et al., 2020). Such reports have collectively led to the hypothesis that SARS-CoV-2 expression in β-cells may potentiate or exacerbate T1D or T2D. However, ACE2 expression in the human pancreas is

only partially characterized, with conflicting results in both the endocrine and exocrine compartments (Fignani et al., 2020; Hikmet et al., 2020; Lee et al., 2020b; Yang et al., 2010; Yang et al., 2020). Indeed, the most cited report (Yang et al., 2010) utilized a single unspecified antibody, was limited in the number of tissue samples and cases, and lacked reagent validation.

To better understand the potential impact of SARS-CoV-2 on diabetes, we performed an extensive investigation of the human pancreas, with particular focus on its endocrine component, the islet of Langerhans. Specifically, we carried out an integration-analysis of publicly available single-cell RNA-sequencing (scRNA-seq) data from isolated human islets, coupled these findings with direct visualization of gene and protein expression of ACE2 using single molecular fluorescence *in situ* hybridization (smFISH), chromogen-based immunohistochemistry (IHC), and performed multicolor immunofluorescence (IF) in human tissue. Importantly, we employed a multi-center approach to the selection, testing and validation of four commercially available ACE2 antibodies by IHC and immunoblot using known ACE2-positive tissues in addition to the pancreas. Finally, we analyzed SARS-CoV-2 nucleocapsid protein (NP) expression in autopsy-derived tissues from individuals with COVID-19 to assess whether the virus was detected in pancreatic islet endocrine cells.

RESULTS AND DISCUSSION

ACE2 and *TMPRSS2* Gene Expression is Low in Human Pancreatic Endocrine Cells.

Diabetes, obesity and advanced age increase the risk of COVID-19 mortality (Zhou et al., 2020). Autopsy studies of individuals infected with SARS-CoV-2 demonstrate systemic viral dissemination with persistence in multiple organs, including the lungs and kidneys (Hanley et al., 2020; Liu et al., 2020; Menter et al., 2020; Wichmann et al., 2020), but there was an apparent limitation of pronounced inflammatory alterations to the lung and reticulo-endothelial system (Dorward et al., 2020). Recent studies (Barron et al., 2020; Fignani et al., 2020; Goldman et al., 2020; Holman et al., 2020; Li et al., 2020; Marchand et al., 2020; Unsworth et al., 2020; Wang et al., 2020) spurred interest in ACE2 expression in the pancreas, particularly the endocrine compartment, to address a potential relationship between diabetes and COVID-19, including the potential for either direct β-cell infection or β-cell damage via indirect mechanisms. To date, studies of ACE2 expression in the pancreas have been limited and contradictory, and analysis of autopsy specimens from COVID-19 cases have not been published, likely due to challenges associated with tissue procurement and post-mortem autolysis.

SARS-CoV-2 entry into cells via the ACE2 receptor requires S protein priming by the mucosal serine proteases (Lee et al., 2020b; Zang et al., 2020). We thus investigated expression patterns of ACE2 and several proteases linked with SARS-CoV-2 processing by conducting an integrated analysis of scRNA-seq data from five public datasets including 22 non-diabetic and 8 T2D individuals (Baron et al., 2016; Grün et al., 2016; Lawlor et al., 2017; Muraro et al., 2016; Segerstolpe et al., 2016). This analysis revealed a low frequency of *ACE2*-expressing cells and low *ACE2* expression levels in the majority of islet cell subsets (**Fig. 1A-B**). In islets from donors without diabetes, *ACE2* was expressed in <2% of endocrine, endothelial and select innate immune cells. *ACE2* was detectable in 4.11% of acinar cells and 5.54% of ductal cells in non-diabetic donors as compared to 8.07% of acinar and 8.13% of ductal cells in

donors with T2D (**Fig. 1A-B,Table S1**). Expression levels of *ACE2* were not different between non-diabetic donors and those with T2D in any of the islet cell subtypes (**Fig. 1A**).

We next investigated the expression patterns of the serine protease, *TMPRSS2*, which is thought to be the main serine protease required for SARS-CoV-2 infectivity. *TMPRSS2* was detectable in 53.73% of acinar and 50.55% of ductal cells in donors without diabetes, and 71.43% of acinar and 58.74% of ductal cells in donors with T2D (**Fig. 1C, Table S1**). Apart from α-cells, which demonstrated 16.55% positivity in non-diabetic donors and 32.07% positivity in donors with T2D, *TMPRSS2* expression was low in the majority of other endocrine cell subsets (**Fig. 1C**). *TMPRSS2* was detectable in 5.46% of β-cells, and neither *ACE2* nor *TMPRSS2* expression differed significantly in β-cells from non-diabetic versus T2D donors (**Fig. 1A,C and S1A,B**). *TMPRSS2* showed higher relative expression levels in ductal and acinar cells compared to β-cells (adjusted $P = 1.31\times10^{-291}$ and $P < 1\times10^{-300}$, respectively), and was detectable in an elevated proportion of these cells in non-diabetic donors ($P < 0.05$) (**Fig. 1C,D**). The frequency and expression of *ACE2* and *TMPRSS2* relative to a subset of cellular identity marker genes across each of the analyzed cell populations highlights, in general, the low expression of *ACE2* and *TMPRSS2* across pancreatic cells (**Fig. 1E**). We also analyzed *ACE2* and *TMPRSS2* levels relative to an expanded list of highly expressed genes in α- and β-cells, including *GCG*, *TTR*, *SCG2*, *INS*, *IAPP*, and *PDX1* (**Fig. 1F,G**).

Because the expression of *ACE2* in combination with an associated protease appears to be required for cellular entry (Lee et al., 2020b; Zang et al., 2020), we calculated the percentage of each cell type that expressed both *ACE2* and *TMPRSS2*. Notably, only 0.24% and 0.10% of α-cells and β-cells were positive for *ACE2* and *TMPRSS2* in islets from donors without diabetes, while no α- or β-cells from donors with T2D expressed both (**Table S2**). Fewer than 4% of acinar and ductal cells in donors without diabetes were positive for *ACE2* and *TMPRSS2*, while co-expression was observed in 8.07% and 6.10% of acinar and ductal cells, respectively in donors with T2D (**Table S2**).

We also investigated expression patterns for other SARS-CoV-2-associated proteases, including *TMPRSS4*, *CTSL*, *ADAM17,* and *TMPRSS11D* (**Table S1** and **Fig. S1C-H**). In addition, we quantitated the percentage of cells that co-expressed *ACE2* and each of these proteases (**Table S2**). *TMPRSS4* was expressed in a similar proportion of α- and β-cells; however, relative expression levels tended to be low in the endocrine pancreas (**Fig. S1C-D**). *CTSL* and *ADAM17* were detected at higher levels in α- and β-cells (**Fig. S1E-F**). The relative expression of *TMPRSS11D* was low in most cell types examined (**Fig. S1G**). Within the β-cells, only *CTSL* showed higher expression in donors with T2D compared to donors without diabetes (adjusted $P = 8.94\times 10^{-32}$, **Fig. S1H**). Notably, less than 1% of β-cells expressed *ACE2* in combination with any of these identified proteases (**Table S2**).

To visualize *ACE2* and *TMPRSS2* mRNA expression patterns *in situ*, we used smFISH on non-diabetic, SARS-CoV-2 negative, "normal" human pancreata from seven donors across a wide age-span (**Table S3**) with duodenum, ileum, and kidney used as positive controls (**Fig. S2A-B**). *ACE2* mRNA was observed in pancreatic ducts, acinar tissue and $CD34^{+}$ endothelial cells (**Fig. 2A,B**), but was observed to a much lesser extent in the islet endocrine cells (**Fig. 2C**). *TMPRSS2* mRNA showed a similar pattern but was expressed at higher frequency (**Fig. 2**). We observed limited expression of *TMPRSS2* and/or *ACE2* in insulin positive β-cells (**Fig. 2C inset**), which was consistent with quantification of *ACE2* and *TMPRSS2* expression and co-expression from scRNA-seq data (**Table S2**). smFISH analysis of other SARS-CoV-2-associated proteases revealed *TMPRSS4* mRNA in the exocrine pancreas, with rare *TMPRSS4* expression within the islet, while *CTSL*, *ADAM17*, and *TMPRSS11D* expression were observed in both the endocrine and exocrine pancreas (**Fig. S2C-F**).

Extensive Reagent Validation Confirms High Level of ACE2 Protein Expression in the Human Pancreas.

Information regarding ACE2 protein expression in pancreatic tissue sections remains limited and unfortunately contradictory. A 2010 study on SARS-CoV and its relationship with diabetes interrogated ACE2 expression in a single donor (43 years of age), with an unspecified antibody, and reported weak ACE2 staining in exocrine tissues but pronounced expression in pancreatic islets (Yang et al., 2010). Fignani and colleagues (Fignani et al., 2020) recently described heterogenous ACE2 expression across donors, pancreatic lobes and islets, and identified three main ACE2-expressing cell types in formalin fixed, paraffin embedded (FFPE) pancreatic sections from seven donors (aged 22-59 years) probed with three ACE2 antibodies (MAB933, ab15348, and ab108252): endothelial cells and pericytes, ductal cells, and in an analysis of 128 islets, β-cells that often presented with a granular staining pattern, partially overlapping with insulin. In contrast, an analysis of tissue microarrays containing pancreatic FFPE sections from 10 donors (aged 30-79 years) utilizing two ACE2 antibodies (MAB933 and HPA000288) reported ACE2 expression restricted to endothelial cells and pericytes and interlobular ducts while ACE2 was not detectable in islets, acinar glandular cells, intercalated ducts, or intralobular ducts (Hikmet et al., 2020). This study, together with a publicly available preprint employing six ACE2 antibodies (Lee et al., 2020a), is noteworthy for the broad range of major human tissues and organs investigated as well as the delineation of mostly shared but also, some distinctive ACE2 antibody staining properties. In light of these diverging observations, it is imperative to utilize multiple ACE2 antibodies on larger donor cohorts to gather a comprehensive description of ACE2 expression in the pancreas.

We selected four widely referenced, commercially available antibodies recognizing specific epitopes and both the short and long isoforms of the ACE2 protein (**Fig. 3A**) (Blume et al., 2020; Ng et al., 2020; Onabajo et al., 2020), to evaluate by immunoblot (**Fig. 3B** and **Fig. S3A-B**) using protein extracts from three non-diabetic, SARS-CoV-2-negative, “normal” pancreas donors (**Table S3**). ACE2 is an 805 amino acid protein (UniProt Q9BYF1) with a theoretical molecular mass of 94.2 kDa but an actual mass of ~120 kDa due to glycosylation at

N-terminus sites (Tipnis et al., 2000). Accordingly, a pronounced ~120kDa band was readily visualized by AF933 and ab108252 while ab15348 and especially MAB933 revealed a much weaker band (**Fig. 3B** and **Fig. S3A**). Nevertheless, in our efforts, all four antibodies demonstrated robust and essentially commensurate staining in human duodenum and kidney FFPE sections (**Fig. S3C**), consistent with two recent reports (Hikmet et al., 2020; Lee et al., 2020a).

We next visualized ACE2 via chromogen-based IHC in FFPE pancreata from non-diabetic, SARS-CoV-2-negative "normal" donors using all four antibodies and consistently observed positive staining in the microvasculature and ductal epithelium (**Fig. 3C**). To further validate specificity, we utilized a peptide-blocking assay wherein ab108252 was pre-incubated with an ACE2 peptide prior to IHC staining (**Fig. S3D**). Taking Western blot and IHC validation into account, ab108252 produced a clearly detectable 120kDa band (**Fig. 3B** and **Fig. S3A**) and crisp *in situ* staining (**Fig. 3C** and **S3C**) that was completely blocked by pre-incubation with the ACE2 peptide (**Fig. S3D**). This is a monoclonal antibody, which offers a high degree of specificity and consistency between lots. Hence, we elected to use ab108252 in subsequent IHC and IF assays.

Human Pancreatic Expression of ACE2 Protein is Primarily Detected in the Duct Epithelium and Microvasculature Across the Lifespan and Positively Associated with Obesity.

To quantitatively evaluate pancreatic ACE2 protein expression, a FFPE tissue cross-section from each of 36 SARS-CoV-2-negative donors without diabetes (aged 0-72 years, **Table S3**) was stained for insulin and ACE2 (ab108252) and scanned to produce a whole-slide image. Co-localization of ACE2 protein with insulin was not observed (**Fig. 3C and Fig. S4A**). The tissue area staining positive for ACE2 was analyzed using the HALO Area Quantification algorithm (**Fig. 4A**). Body mass index (BMI)-matched donors were binned into six age groups: neonate (0-

0.25 years, *n* = 6), infant and toddler (0.25-2 years, *n* = 6), child (2-11 years, *n* = 6), adolescent (11-15 years, *n* = 6), young adult (20-33 years, *n* = 6), and senior adult (51-72 years, *n* = 6). Collectively, these data demonstrated the percentage of tissue staining positive for ACE2 increased steadily from birth throughout childhood, peaking in adolescence and maintained through early adulthood, followed by a decline in persons over 50 years of age (**Fig. 4B**). The ACE2-positive area did not appear different for male versus female subjects (**Fig. 4B**), but with *n* = 6 per age group, statistical analysis was not performed and will be the subject of future efforts.

Obesity is associated with an increased risk of COVID-19-associated morbidity and mortality (Hussain et al., 2020; Nakeshbandi et al., 2020; Tartof et al., 2020). Taneera and colleagues (Taneera et al., 2020) observed no relationship between *ACE2* and BMI in isolated pancreatic islets analyzed by microarray. To analyze this *in situ*, we examined ACE2 protein expression in the aforementioned six young adult donors together with pancreata from 16 additional donors (20-33 years of age, SARS-CoV-2 negative, no diabetes, for a total *n* = 22) with BMI ranging from normal (19.5 kg/m^2) to obese (35.6 kg/m^2) (**Table S3**). Notably, we observed a positive correlation between ACE2 positive area and BMI (**Fig. 4C**).

To more precisely visualize pancreatic ACE2 localization, we performed IF staining for ACE2 (again using ab108252) in conjunction with insulin and glucagon (**Fig. 4D-F** and **Fig. S4B**) or with CD34 (**Fig. S4C**). Across all ages, we observed ACE2 expression in the pancreatic ductal epithelium (**Fig. 4D**) but not major blood vessels (**Fig. S4B**), based on their morphology and geographic positioning. ACE2 was highly expressed in the microvasculature within acinar and islet regions, with no evidence of α-cells or β-cells expressing ACE2 protein (**Fig. 4E,F** and **Fig. S4A,C**). Our data corroborate findings by two groups (Coate et al., 2020; Hikmet et al., 2020), yet contrast with two others (Fignani et al., 2020; Yang et al., 2010). Moreover, our IHC analyses do not support the notion that islet endocrine cells may preferentially express a recently described short ACE2 isoform (Fignani et al., 2020). Beyond this, we note that this

isoform lacks the SARS-CoV-2 binding domain (Blume et al., 2020; Ng et al., 2020; Onabajo et al., 2020) and thus, would not render endocrine cells susceptible to infection. These disparate results may be influenced by technical (e.g., tissue processing, antigen retrieval, reagent), material (e.g., isolated islets versus tissue sections), or donor differences. However, in aggregate, our analysis of 52 donors across a wide age and BMI range provides a comprehensive perspective on pancreatic ACE2 protein distribution that demonstrates limited to no ACE2 expression by pancreatic endocrine cell types, including β-cells (**Fig. 3** and **Fig. 4**), corroborating scRNA-seq and smFISH gene expression data (**Fig. 1** and **Fig. 2**).

SARS-CoV-2 NP is Localized to Pancreatic Ductal Epithelium from COVID-19 Cases With and Without T2D.

Following autopsy, we reviewed pancreatic pathology by hematoxylin and eosin (H&E)-stained sections in three individuals with fatal COVID-19 (aged 45-72 years, **Fig. 5A-C**), two of whom had a previous diagnosis of T2D (**Table S4**). Case 1, was an individual without history of diabetes. The major findings included severe fatty replacement of acinar cell mass and moderate arteriosclerosis (**Fig. 5A**). Lobules contained fibrotic centers with residual acinar cells and islets surrounding ductules (**Fig. 5A insert)**. Islets were observed primarily within fibrotic regions. Case 2 was an individual with T2D whose pancreas had moderate fatty replacement and limited centrolobular fibrosis (**Fig. 5B**). Dystrophic calcification of adipocytes was rare. We observed numerous islets and one microthrombus without adjacent hemorrhage (**Fig. 5B insert**). The pancreas of another individual with T2D (Case 3) showed mild to moderate arteriosclerosis with acinar regions containing mild centrolobular fibrosis (**Fig. 5C**). Moderate numbers of islets were present of varying sizes (**Fig. 5C insert**). None of these individuals showed islet amyloidosis or acute polymorphonuclear cell infiltrates. These histopathological findings were compatible with the normal range of expected lesions within the exocrine compartment in pancreata from aged persons and those with T2D.

IHC showed islets containing insulin-positive (INS+) β-cells with mostly spherical profiles, small to medium sizes, and varying proportions of β- to α-cells in all three cases (**Fig. 5D**). We observed numerous single and clustered INS+ and glucagon-positive (GCG+) cells in ductules of fibrotic foci. The endothelium showed moderate ACE2 staining intensity within both endocrine and exocrine compartments. The ductal epithelium showed low to moderate ACE2 staining intensity throughout the cytoplasm (**Fig. S5A**) similar to that observed in non-diabetic pancreas donors (**Fig. 3C**).

IHC for SARS-CoV-2 NP was also conducted to investigate the cellular distribution of the virus. A lung sample from a person with COVID-19 pneumonia was used to optimize staining conditions. Immunopositive alveolar epithelial cells and macrophages were observed with numerous viral inclusions (**Fig. S5B**). In COVID 19 Case 1 SARS-CoV-2 NP was present in some intralobular and interlobular ductal epithelial cells shown near an islet and widely scattered throughout the exocrine regions (**Fig. 5E,F** and **Fig. S5C,D**). Pancreata from Case 2 and 3, who had T2D, showed little to no immunopositivity for SARS-CoV-2 NP.

We believe these data provide an important foundation for considerations of pancreatic SARS-CoV-2 infection as a potential trigger for diabetes. Indeed, the notion of ACE2 expression on pancreatic β-cells as a potential mechanism linking the two conditions may, in our view, promote a quasi-dogmatic perspective (The Lancet Diabetes Endocrinology, 2020) that is grounded in limited experimental evidence (Yang et al., 2010). However, the histopathology data presented herein do not support a simple model of direct and widespread islet endocrine, including β-cell infection via the ACE2 receptor. Rather, preferential ACE2 gene and protein expression in microvascular and ductal structures suggest these cells constitute a more likely target for viral infection, a notion that is in principle supported by our observation of very limited SARS-CoV-2 NP expression in ductal epithelium but not islet endocrine cells of pancreata from individuals with COVID-19. While scarce ACE2 protein expression and limited SARS-CoV-2 propagation, as most recently documented for the lung (Hönzke et al., 2020), does not preclude extensive tissue damage mediated by innate

immune responses in particular, the absence of polymorphonuclear infiltrations in the three COVID-19 pancreata interrogated here indicates a very limited degree of inflammation consistent with that reported for many tissues other than the lung and reticulo-endothelial system (Dorward et al., 2020). More detailed investigations of pancreatic tissue from fatal COVID-19 cases, to date a very limited resource, will be necessary to answer outstanding questions about the potential pathological involvement of the pancreas in COVID-19.

Limitations of Study

Our delineation, localization and quantification of pancreatic ACE2 is largely based on *in silico* and *ex vivo in situ* analyses of gene (public scRNA-seq data, smFISH) and protein (IHC, IF) expression in pancreata of a broad cohort of organ donors without diabetes and a more limited number of organs collected from COVID-19 autopsy subjects. As such, our pancreatic tissue analyses can only provide approximate predictions regarding ACE2 protein expression in isolated islets and islet cells or their susceptibility to *in vitro* SARS-CoV-2 infection. Although the aggregate scRNA-seq data demonstrates relatively little *ACE2* mRNA in endocrine cells, Yang et al., in a wide-ranging report on the development of a stem cell-based platform for SARS-CoV-2 infection studies, recently demonstrated both ACE2 protein expression by endocrine cells in isolated human islets and their productive infection with SARS-CoV-2 (Yang et al., 2020). Without question and in addition to stem cell-derived endocrine cells and islet organoids, isolated human islets constitute an important model system for research discovery. Further work will be needed to precisely quantify the fractions and expression levels of ACE2 by islet endocrine cells in these islet preparations, to evaluate possible modulation of ACE2 by the prolonged and varied islet handling requirements (e.g., isolation, culture under different conditions, dispersion), to define the exact role of ACE2 in mediating SARS-CoV-2 infection *in vitro* and *in vivo* using extended islet xenotransplantation approaches, and to interrogate the precise relation of scarce ACE2 expression and immunopathology as most recently demonstrated for the lung in a manuscript available for public review (Hönzke et al., 2020). Beyond

this, contrasting epidemiological reports from the United Kingdom and Germany (Tittel et al., 2020; Unsworth et al., 2020) not only underscore the requirement for data on diabetes incidence and SARS-CoV-2 infection rates in defined populations over time, but in addition, raise the need for studying pancreatic tissues from donor cohorts of different demographics, ethnicities, and geographic populations. Indeed, it is possible that COVID-19 may cause an upregulation of ACE2 in endocrine or other cell types, but as of yet, gene and protein expression levels cannot be reliably quantified from autopsy tissues due to pancreatic autolysis and the relative scarcity of high-quality pancreas tissues obtained from SARS-CoV-2 infected individuals. Only in the larger context of expanded investigations into pancreatic histopathology of individuals with COVID-19, with carefully controlled *in vitro* infection studies, judicious use of animal models to directly test the ability of SARS-CoV-2 to infect the endocrine pancreas, and crucially, a balanced assessment of emerging and future epidemiological studies (DiMeglio et al., 2020) can we provide a complete framework for an informed assessment of diabetes risk and potential prevention in the wake of SARS-CoV-2 infection.

SUPPLEMENTAL INFORMATION

Supplemental Information includes 5 Figures and 4 Tables, and can be found with this article at <Provided by *Cell Metabolism*>.

ACKNOWLEDGEMENTS

We thank the families of the organ donors and autopsy subjects for the gift of tissues. We also thank Jill K. Gregory, CMI (Icahn School of Medicine at Mount Sinai, New York, New York) for preparing the graphical abstract.

AUTHOR CONTRIBUTIONS

IK researched data, generated figures, and wrote the manuscript; WW, FS, VvdH, MJ, PJ, XT, ECJ, and CY researched data and reviewed/edited the manuscript; HN generated figure 2A, contributed to discussion, and reviewed/edited the manuscript, JLH and JDP reviewed pathology and reviewed/edited the manuscript, ALP contributed to discussion and wrote the manuscript; RL, SC, and AP contributed to discussion and reviewed/edited the manuscript, RSVH procured COVID-19 autopsy tissues, reviewed pathology, and reviewed/edited the manuscript, MCT reviewed pathology and wrote the manuscript, CEM, DH, and MAA conceived of the study and wrote the manuscript.

DECLARATION OF INTERESTS

The authors declare no competing interests.

Funding. These efforts were supported by NIH P01 AI042288 and UC4 DK108132 (MAA), JDRF (MAA); NIH R01 DK122160 (MCT); NIH R01 AI134971 and P30 DK020541 (DH); JDRF 3-PDF-2018-575-A-N (VvdH); R01 DK093954, R21 DK119800-01A1, UC4 DK104166 and U01 DK127786 (CEM), VA Merit Award I01BX001733 (CEM), Imaging Core of NIH/NIDDK P30

DK097512 (CEM), gifts from the Sigma Beta Sorority, the Ball Brothers Foundation, and the George and Frances Ball Foundation (CEM); the Network for Pancreatic Organ donors with Diabetes (nPOD; RRID:SCR_014641) (5-SRA-2018-557-Q-R); and The Leona M. & Harry B. Helmsley Charitable Trust (2018PG-T1D053). The authors also wish to acknowledge the Islet and Physiology Core of the Indiana Diabetes Research Center (P30DK097512). The funders had no role in study design, data collection and interpretation, or the decision to submit the work for publication.

FIGURE LEGENDS

Fig. 1. SARS-CoV-2 associated gene expression in isolated human pancreatic islets, Related to Table S1, Table S2, and Fig. S1

(A) Bar graph showing the percentage of cells with detectable *ACE2* in islets from pancreata of donors with (n = 2,705 cells) and without type 2 diabetes (n = 12,185 cells).

(B) Violin plot showing the distribution of *ACE2* normalized expression in islet cells from pancreata of donors without diabetes.

(C) Bar graph showing the percentage of cells with detectable *TMPRSS2* in islets isolated from pancreata of donors with (n = 2,705 cells) and without type 2 diabetes (n = 12,185 cells); *adjusted $P < 0.05$, paired Student's t-test for indicated comparisons.

(D) Violin plot showing the distribution of *TMPRSS2* normalized expression in islets cells from pancreata of donors without diabetes; ***adjusted $P < 0.001$, Wilcoxon rank sum tests. Bonferroni corrections were used to adjust for multiple comparisons.

(E) Dot plot of *ACE2* and *TMPRSS2* expression compared with cell type-enriched genes in islets from pancreata of donors without type 2 diabetes (n = 12,185 cells). The size of each dot indicates the percentage of cells in a given population expressing the indicated gene. The dot color represents the scaled average expression.

(F) Violin plot showing the relative expression of *ACE2* and *TMPRSS2* in islet α-cells from pancreata of donors without diabetes (n = 3,770 cells) compared with select α-cell-enriched genes.

(G) Violin plot showing the relative expression of *ACE2* and *TMPRSS2* in islet β-cells from pancreata of donors without diabetes (n = 2,985 cells) compared with select β-cell-enriched genes.

Fig. 2. Single molecular fluorescent in situ hybridization based validation of SARS-CoV-2 associated gene expression in human pancreas, Related to Fig. S2.

(A) Representative images of smFISH for *ACE2* and *TMPRSS2* mRNA in human pancreatic tissue sections counterstained for insulin. Inset highlights mRNA distribution in pancreatic ducts; scale bars: 20µm. The lower image is a high magnification of the boxed region in the merged panel.

(B) Representative smFISH images showing the presence of *ACE2* and *TMPRSS2* in CD34-positive cells in human pancreatic tissue sections; scale bars: 10µm. The lower image is a high magnification of the boxed region in the merged panel.

(C) Representative images of smFISH for *ACE2* and *TMPRSS2* mRNA in human pancreatic tissue sections counterstained for insulin. Inset highlights distribution in the endocrine pancreas; scale bars: 20µm. The lower image is a high magnification of the boxed region in the merged panel.

Fig. 3. ACE2 protein is readily detected in normal human pancreas with its expression largely restricted to ductal and microvascular structures, Related to Table S3 and Fig. S3 and Fig. S4.

(A) ACE2 protein structure illustrating the location of respective antibody directed antigen sites: SP, signal peptide; TM, transmembrane domain; CD, cytoplasmic domain.

(B) Immunoblot analysis of four commercially available ACE2 antibodies using total pancreas lysates from three control organ donors (p1-p3) with accompanying Actin labeling. 120 and 37 indicate the molecular weight (in kDa) of ACE2 and Actin, respectively.

(C) Representative IHC images of human pancreas tissue sections stained for ACE2 and insulin using four commercially available ACE2 antibodies. Scale bars: 200 µm. Abbreviations: d, duct; mv, microvasculature.

Fig. 4. ACE2 protein expression is evident in normal pancreata throughout the human lifespan and correlates with BMI, Related to Table S3 and Fig. S4.

(A) Scheme of the experimental setup illustrating human pancreatic tissue processing, whole-stained slide imaging and machine learning algorithm application for the generation of ACE2 protein expression data.

(B) Quantification of ACE2 protein expression in the pancreas of male (blue) and female (orange) control organ donors with ages ranging from birth to 72 years shows progressive developmental changes. Data were analyzed by one-way ANOVA and Tukey's post hoc test for multiple comparisons and are presented as a percentage.

(C) Quantification of ACE2 protein expression in the pancreas of male (blue) and female (orange) control organ donors with BMI ranging from normal to obese, r = 0.81, n = 22, P < 0.001.

(D) Representative confocal images (from n = 14) of ACE2 protein expression in pancreatic ducts of control donors across the different age groups indicated. Scale bars (left to right): 100µm, 200µm, 200µm, 300µm, 300µm, 300µm.

(E) Representative immunofluorescence images (n = 14) show ACE2 protein expression in pancreatic microvasculature from control donors across different age groups. Scale bars: 100µm.

(F) Representative immunofluorescence images (n = 14) of pancreatic islets showing ACE2 protein expression restricted to the islet's microvasculature in pancreata from control organ donors across different age groups. Scale bars: 50µm.

Fig. 5. Pathological changes in pancreata of individuals with COVID-19, Related to Table S4 and **Fig. S5C-D.**

(A) Pancreas tissue section from COVID-19 Case 1 stained for H&E. Inset highlights fibrotic center with residual acinar cells and islet surrounding ductules. Scale bars: 3mm, inset 200µm.

(B) Pancreas tissue section from COVID-19 Case 2 stained for H&E. Inset highlights microthrombus without adjacent hemorrhages. Scale bars: 3mm, inset 200µm.

(C) Pancreas tissue section of COVID-19 Case 3 stained for H&E. Inset highlights a large, irregularly shaped pancreatic islet surrounded by fibrotic tissue. Scale bars: 3mm, inset 200µm.

(D) Representative pancreas tissue sections from three COVID-19 cases stained for ACE2, insulin (INS) and glucagon (GCG). Scale bars: 200µm.

(E) SARS-CoV-2 NP observed in intralobular ducts (d) near an islet in the pancreas of COVID-19 Case 1. Scale bars: 10µm.

(F) Representative image of multiple ducts showing SARS-CoV-2 NP positivity in the pancreas of COVID-19 Case 1. d; duct. Scale bar: 20µm.

STAR METHODS

RESOURCE AVAILABILITY

Lead Contact

Further information and requests for reagents may be directed to and will be fulfilled by the lead contact/corresponding author, Mark A. Atkinson (atkinson@ufl.edu).

Materials Availability

This study did not generate new unique reagents. Tissues used in this study were obtained from the Network for Pancreatic Organ donors with Diabetes (nPOD) and from autopsies performed on deceased individuals with COVID-19. nPOD tissues are freely available to approved investigators following successful application to the nPOD Tissue Prioritization Committee (TPC).

Data and Code Availability

This study did not generate code. Single cell sequencing data were obtained from the Gene Expression Omnibus (GEO) Repository: GSE84133 (Baron et al., 2016), GSE81076 (Grün et al., 2016), GSE85241 (Muraro et al., 2016), and GSE86469 (Lawlor et al., 2017), as well as from ArrayExpress: accession number E-MTAB-5061 (Segerstolpe et al., 2016). Original histology and additional de-identified organ donor data are available from nPOD at the nPOD online digital pathology database and from the corresponding author upon reasonable request.

EXPERIMENTAL MODEL AND SUBJECT DETAILS

nPOD Donors and Sample Processing

Transplant-quality pancreas, duodenum, and kidney were recovered by JDRF nPOD (www.jdrfnpod.com) from 56 COVID-19 negative organ donors without diabetes (**Table S3**) according to established protocols and procedures (Campbell-Thompson et al., 2012), as approved by the University of Florida Institutional Review Board (201400486), the United

Network for Organ Sharing (UNOS), and according to federal guidelines with informed consent obtained from each donor's legal representative. Organs were shipped in transport media on ice via organ courier to the nPOD Organ Pathology and Processing Core (OPPC) at the University of Florida where tissues were processed (Campbell-Thompson et al., 2012). Medical chart and medical-social questionnaire reviews were performed, and T1D-associated autoantibodies measured by ELISA (Wasserfall et al., 2016) to confirm non-diabetic health status. Donor demographics, hospitalization duration, and organ transport time were determined from hospital records or UNOS. This study was not powered to statistically assess associations between ACE2 localization and donor sex.

Autopsy Subjects and Sample Processing

Pancreas was recovered from three individuals who tested positive for SARS-CoV-2 by reverse transcription polymerase chain reaction (RT-PCR) test within 24-48 hours of death at the University Medical Center New Orleans (New Orleans, LA), which is equipped with an autopsy suite that meets U.S. Centers for Disease Control and Prevention standards for autopsy of persons with COVID-19 (**Table S4**). Consent for autopsy without restriction was given by next of kin, and the studies within this report were determined to be exempt from oversight by the Institutional Review Board at Louisiana State University Health Sciences Center.

METHOD DETAILS

Single-Cell RNA-Sequencing Data Analysis

Five human islet scRNA-seq datasets were obtained from publicly available repositories. These included four datasets from the Gene Expression Omnibus (GEO) Repository: GSE84133 (inDrop) (Baron et al., 2016), GSE81076 (Celseq) (Grün et al., 2016), GSE85241 (CelSeq2) (Muraro et al., 2016), and GSE86469 (Fluidigm C1) (Lawlor et al., 2017). In addition, we analyzed an ArrayExpress database under the accession number E-MTAB-5061 (SMART-Seq2) (Segerstolpe et al., 2016). For all scRNA-seq datasets, the same initial normalization was

performed: gene expression values for each cell were divided by the total number of transcripts and multiplied by 10,000. Following log-transformation, cells were filtered that expressed fewer than 500 genes/cell (InDrops), 1,750 genes/cell (CelSeq), or 2,500 genes/cell (CelSeq2, Fluidigm C1, and SMART-Seq2) in accordance with the methods employed in the original corresponding publications, leaving 14,890 cells in total for the combined analysis. Pancreatic islet cell subtypes were identified using methods outlined in (Butler et al., 2018).

To integrate scRNA-seq data, we applied canonical correlation analysis (CCA) in Seurat v.3 (Butler et al., 2018) using "FindIntegrationAnchors" and "IntegrateData" functions. We chose the top 2,000 variable genes from each dataset to calculate the correlation components (CCs) and "FindClusters" was utilized for shared nearest neighbor (SNN) graph-based clustering. Clusters were visualized with t-distributed stochastic neighbor embedding (t-SNE) by running dimensionality reduction with "RunTSNE" and "TSNEPlot". To compare the average gene expression within the same cluster between cells of different samples, we applied the AverageExpression function. Statistical analyses are further described in QUANTIFICATION AND STATISTICAL ANALYSIS below. Violin plots (VlnPlot) were used to visualize gene expression levels (**Fig. 1B, D, F, G** and **Fig. S1)**. The "DotPlot" function was used to visualize *ACE2* and TMPRSS2 expression levels compared with cell type-enriched genes (**Fig. 1E)**.

Single Molecular Fluorescent In-Situ Hybridization

To define mRNA expression patterns of SARS-CoV-2 associated genes in human pancreata, smFISH was performed using the RNAscope® Multiplex Fluorescent V2 kit (Advanced Cell Diagnostics, Newark, CA) in FFPE tissue cross-sections (5µm) from seven non-diabetic, SARS-CoV-2 negative human organ donors from nPOD (**Table S3, Fig. 2A-C,** and **Fig. S2C-F**). Slides were baked at 60°C for 1 hour, followed by dehydration with xylene for 5 minutes x 2 and 100% ethanol for 2 minutes at room temperature (RT). Next, slides were air dried at 60°C for 5 minutes, treated with hydrogen peroxide for 10 minutes at RT, and washed 4 times with ddH_2O,

followed by antigen-retrieval at 99°C for 15 minutes. After another wash with ddH_2O at RT for 15 seconds, slides were incubated at 100% ethanol for 3 minutes, air dried and then treated with protease plus for 30 minutes at 40°C. Next, slides were hybridized with RNAscope® Probes for *TMPRSS2, TMPRSS4, TMPRSS11D, CTSL, ADAM17* and *ACE2* mRNA, and detected using secondary TSA plus fluorophores (1:1500 dilution) according to the manufacture's protocol (Perkin Elmer, Waltham, MA). Slides were immediately washed with 1X PBS and PBS containing 2% FBS for 5 minutes, blocked with donkey serum for 30 minutes, and incubated with ready to use (RTU) guinea pig polyclonal anti-insulin (no dilution; Agilent Santa Clara, CA) and/or mouse monoclonal anti-CD34 antibody (1:1,000 dilution, Novus Biologicals) overnight. The following morning, slides were washed with 1X PBS and PBS containing 2% FBS for 5 minutes and probed using either Alexa Fluor (AF)-488 goat anti-guinea pig IgG (1:500 dilution, Invitrogen, Carlsbad, CA) or AF-488 donkey anti-mouse IgG (1:1,000 dilution, Invitrogen) secondary antibodies. Finally, the slides were washed with PBS, counterstained with DAPI, and mounted with a coverslip using ProLong™ Gold antifade mounting media (Thermo Fisher, Rockford, IL). Images were acquired using an LSM800 confocal microscope (Carl Zeiss, Germany).

Tissue Homogenization

Pancreas tissues were homogenized in modified radioimmunoprecipitation (RIPA) buffer (50 mM Tris-HCl pH 7.4, 150 mM NaCl, 5 mM EDTA, 1 mM EGTA, 1% NP-40, 0.5% sodium deoxycholate and 0.1% SDS) with freshly prepared protease and phosphatase inhibitor cocktails (Thermo Fisher Scientific) using a Tissue Tearor (BioSpec Inc., Bartlesville, OK). After homogenization, tissue was further disrupted with a Vibra-Cell™ sonicator (Sonics & Materials Inc., Newtown, CT) for 15 seconds, placed on ice for 15 minutes, then sonicated again and placed on ice for another 15 minutes. The tissue homogenates were centrifuged at 14,000 x *g*

for 20 minutes at 4°C, and the supernatants were assayed for total protein concentration using a Pierce™ BCA Assay kit (Thermo Fisher Scientific) and stored at -80°C until use.

Western Blotting

Fifty micrograms of protein lysates in Laemmli's buffer containing 2.5% β-mercaptoethanol were boiled at 100°C for 5 minutes prior to loading into a 4-20% gradient Mini-PROTEAN TGX™ Stain-Free gel (Bio-Rad, Hercules, CA). After protein separation, gels were activated using a Gel DOC™ EZ imager (Bio-Rad), then transferred onto nitrocellulose membranes (LI-COR Biosciences, Lincoln, NE). Following protein transfer, membranes were scanned with the Gel DOC™ EZ imager, and total protein staining was visualized and quantified using Image Lab software version 5.2.1 (Bio-Rad). Then, membranes were washed and blocked for 1 hour at RT with Intercept™ Blocking Buffer (LI-COR Biosciences). Thereafter, the membranes were incubated at 4°C overnight with one of four primary antibodies (rabbit monoclonal anti-ACE2 (1:1,000 dilution, Abcam, Cambridge, MA), rabbit polyclonal anti-ACE2 (1:500 dilution, Abcam), mouse monoclonal anti-ACE2 (1:1,000 dilution, R&D Systems), goat polyclonal anti-ACE2 (1:500 dilution, R&D Systems, Minneapolis, MN)) and mouse monoclonal anti-β-actin (1:10,000 dilution; Sigma-Aldrich, St. Louis, MO) in Intercept™ Antibody Diluent (LI-COR Biosciences). The membranes were then washed with Tris-buffered saline containing 0.1% Tween 20 (TBST) three times at 5 minute intervals, incubated with secondary antibodies (IRDye 800CW goat anti-rabbit IgG (1:30,000 dilution), IRDye 800CW goat anti-mouse IgG (1:30,000 dilution), IRDye 800CW donkey anti-goat IgG (1:30,000 dilution), or IRDye 680LT donkey anti-mouse (1:40,000 dilution), all from LI-COR Biosciences) for 1 hour at RT. The membranes were washed three times with TBST at 5-minute intervals. Immunoreactive bands were visualized and densitometrically analyzed using Odyssey infrared scanner and Image Studio software version 3.1 (LI-COR Biosciences) (**Fig. 3B** and **Fig. S3A-B**).

Immunohistochemistry

FFPE pancreas, duodenum, and kidney tissues were sectioned (4μm), deparaffinized,

rehydrated by serially passing through changes of xylene and graded ethanol, subjected to heat induced antigen retrieval in 10mM Citra pH 6, and blocked with avidin, biotin, and goat serum. For single-stained kidney and duodenum tissue sections (**Fig. S3C**) and for SARS-CoV-2 NP single stained lung and pancreas sections (**Fig. 5E-F** and **Fig. S5B-C**), slides were incubated overnight at 4^{o}C with one of four primary antibodies against ACE2 (rabbit monoclonal anti-ACE2, 1:200 dilution (Abcam); rabbit polyclonal anti-ACE2, 1:2,000 dilution (Abcam); mouse monoclonal anti-human ACE2, 1:100 dilution, (R&D Systems); goat polyclonal anti-ACE2, 1:100 dilution, (R&D Systems)) or a primary antibody against SARS-CoV-2 NP (mouse monoclonal anti-SARS-CoV-2 NP, 1:50 dilution, Invitrogen). Slides were washed, then incubated for 30 minutes at RT with biotinylated secondary antibodies (biotinylated goat anti-rabbit IgG, 1:200 dilution (Vector Laboratories, Burlingame, CA); biotinylated horse anti-mouse IgG, 1:200 dilution (Vector Laboratories); biotinylated rabbit anti-goat, 1:200 dilution (Vector Laboratories)), and developed with ImmpactDAB (Vector Laboratories) followed by hematoxylin counterstain.

For peptide blocking experiments (**Fig. S3D**) the primary antibody (monoclonal rabbit anti-ACE2, 1:100 dilution (Abcam)) was incubated with 1mg/mL ACE2 peptide (Abcam) for one hour at RT, before applying to pancreas slides for overnight incubation at 4^{o}C. Thereafter, IHC methodology was carried out as described for single stained sections.

For double- and triple-stained slides, FFPE pancreas slides were prepared for heat induced antigen retrieval in Borg Decloaker RTU (BioCare Medical, Pacheco, CA) followed by 3% H_2O_2. After washing, tissues were blocked with Background Sniper (BioCare Medical) followed by staining. For insulin and ACE2 double-staining (**Fig. 3C, Fig. 4A** and **Fig. S4B**), blocked slides were incubated for 20 minutes at RT with the first primary antibody (rabbit monoclonal anti-ACE2, 1:200 dilution (Abcam)), then washed and incubated with MACH 2 Double Stain Kit 1 (BioCare Medical) for 20 minutes at RT. Slides were washed and developed using DAB Chromogen solution (BioCare Medical), then subjected to a second round of heat-induced antigen retrieval in Borg Decloaker RTU, followed by 3% H_2O_2. After washing, slides

were again blocked with Background Sniper, washed, and incubated with the second primary antibody (rabbit monoclonal anti-insulin, 1:2,000 dilution (Abcam)) for 30 minutes at RT. After washing, slides were incubated with MACH 2 Double Stain Kit 2 for 30 minutes at RT, washed, and developed with Warp Red Chromogen solution (BioCare Medical) followed by Hematoxylin counterstain. For SARS-CoV-2 NP and cytokeratin 19 double-staining (**Fig. S5D**), slides were incubated with primary antibody against SARS-CoV-2 NP (mouse monoclonal anti-SARS-CoV-2 NP, 1:50 dilution, Invitrogen overnight. Slides were washed, then incubated for 30 minutes at RT with biotinylated secondary horse anti-mouse IgG, 1:200 dilution (Vector Laboratories) and developed with ImmpactDAB (Vector Laboratories). Next, slides were subjected to a second round of heat-induced antigen retrieval in Borg Decloaker RTU, followed by 3% H_2O_2. After washing, slides were again blocked with Background Sniper, washed, and incubated with the second primary antibody (mouse monoclonal anti-cytokeratin 19, 1:50 dilution, Agilent) for 3 minutes at RT. After washing, slides were incubated with MACH 2 Double Stain Kit 1 for 20 minutes at RT, washed, and developed with Ferangi Blue Chromogen solution (BioCare Medical).

For ACE2, insulin and glucagon triple-staining (**Fig. 5D**), blocked slides were incubated for 20 minutes at RT with a primary antibody cocktail (mouse monoclonal anti-glucagon, 1:1,000 dilution (Abcam) plus rabbit monoclonal anti-ACE2, 1:200 dilution (Abcam)), then washed and incubated with MACH 2 Double Stain Kit 1 (BioCare Medical) for 20 minutes at RT. Slides were washed and developed using DAB Chromogen solution for ACE2 visualization followed by Ferangi Blue Chromogen solution (BioCare Medical) for glucagon visualization. Slides were then subjected to a second round of heat-induced antigen retrieval in Borg Decloaker RTU, followed by 3% H_2O_2. After washing, slides were again blocked with Background Sniper, washed, and incubated with the third primary antibody (rabbit monoclonal anti-insulin, 1:2,000 dilution (Abcam)) for 30 minutes at RT. After washing, slides were incubated with MACH 2 Double Stain Kit 2 for 30 minutes at RT, washed, and developed with Warp Red Chromogen

solution (BioCare Medical) followed by Hematoxylin counterstain.

Following single-, double-, or triple-IHC staining, whole slides were scanned at an absolute magnification of 20x using an Aperio CS2 Scanscope (Leica/Aperio, Vista, CA), and stored in the nPOD online digital pathology database (eSLIDE version 12.4.0.5043, Leica/Aperio). Images were taken using Aperio ImageScope v12.4.3 or a Keyence BZ-X700 microscope.

Immunofluorescence

For immunofluorescence staining, FFPE pancreas sections were sectioned (4µm), deparaffinized, and rehydrated with antigen retrieval in 10mM Citra pH 6 and blocking as described above for IHC. Slides were incubated overnight at 4^{o}C with primary antibodies: a) monoclonal rabbit anti-ACE2 (1:100 dilution; Abcam), polyclonal guinea pig anti-insulin RTU antibody (undiluted; Agilent), and monoclonal mouse anti-glucagon (dilution; 1:20,000 Abcam) (**Fig. 4D-F**) or b) monoclonal rabbit anti-ACE2 (1:100 dilution; Abcam) and monoclonal mouse anti-CD34 (dilution 1:1,000; Novus Biologicals, Centennial, CO) (**Fig. S4C**). Slides were washed, then incubated for 45 minutes at RT in the dark with secondary antibodies: a) goat anti-rabbit IgG-AF555, goat anti-mouse IgG-AF488, and goat anti-guinea pig IgG-AF647, or b) goat anti-rabbit IgG-AF594 and goat anti-mouse IgG-AF488 (all from Invitrogen). Slides were washed, then counterstained with DAPI and viewed using a Keyence BZ-X700 automated fluorescence microscope.

H&E Staining

H&E staining was performed on FFPE pancreas tissues sections (4µm) from the three COVID-19 autopsy subjects according to standard methodology. Whole slides were scanned using an Aperio CS2 Scanscope (Leica/Aperio, Vista, CA), and stored in the nPOD online digital pathology database (eSLIDE version 12.4.0.5043, Leica/Aperio). Images were taken using Aperio ImageScope v12.4.3.

QUANTIFICATION AND STATISTICAL ANALYSIS

For scRNA-seq analysis, *n* represents the number of cells as indicated in the figure legends. Analyses were performed in R as described in METHOD DETAIL above. Differences in the average gene expression levels between pancreatic cell subsets or within each cell subset from non-diabetic donors versus donors with T2D were compared using Wilcoxon rank sum tests, requiring a minimum 1.19-fold change between the two groups and expression in at least 10% of cells from either group. Bonferroni corrections were used to adjust for multiple comparisons. Paired Student's *t*-tests were used to compare proportions of cells with detectable gene expression. *P* values < 0.05 were considered significant. Violin plot limits show maxima and minima, and the dots represent individual data points. smFISH data were not quantitatively evaluated. For the quantification of ACE2 protein expression throughout the human lifespan and for the analysis of correlation between ACE2 protein expression and BMI, digitized images of ACE2 and insulin co-stained slides were analyzed using the HALO quantitative image analysis platform V3.0.311.262 (Indica Labs, Inc, Corrales, NM) (**Fig. 4A**). The annotation pen tool was used to outline the tissue section to determine total tissue area (mm^2). The Area quantification algorithm v2.1.3 based on red, blue, green (RBG) spectra was employed to detect ACE2 positive tissue area stained for 3,3'-Diaminobenzidine (DAB, brown). The algorithm detected DAB IHC positivity and calculated percentage of ACE2 positive area per total tissue area. For the ACE2 expression as factor of age study, BMI-matched donors (*n* = 36) were binned into six age groups representing major stages of human life: neonatal (0-0.25 years), infant and toddler (0.25-2 years), childhood (2-11 years), puberty (11-15 years), young adult (20-33 years), and senior adult (51-72 years). Data were analyzed in GraphPad Prism v8.3 (GraphPad Software, San Diego, CA) by one-way ANOVA followed by Tukey's post hoc test for multiple comparisons with significance defined as *P* < 0.05 and graphed with the median percent ACE2 area shown for each group in a box and whisker plot. To assess for an association between ACE2 expression and BMI, we reviewed the 34 nPOD donors aged 20-33 years without diabetes with

samples available and selected those without significant underlying pancreatic pathology. This resulted in evaluation of 22 adult organ donors with BMI ranging from 19.5-35.6 kg/m^2; data were analyzed in R using Spearman's correlation test. All image analysis data were collected in blinded fashion. The remaining IF and IHC data were not quantitatively evaluated.

REFERENCES

Baron, M., Veres, A., Wolock, S., Faust, A., Gaujoux, R., Vetere, A., Ryu, J., Wagner, B., Shen-Orr, S., Klein, A., et al. (2016). A Single-Cell Transcriptomic Map of the Human and Mouse Pancreas Reveals Inter- and Intra-cell Population Structure. Cell systems *3*, 346-360.e344.

Barron, E., Bakhai, C., Kar, P., Weaver, A., Bradley, D., Ismail, H., Knighton, P., Holman, N., Khunti, K., Sattar, N., et al. (2020). Associations of type 1 and type 2 diabetes with COVID-19-related mortality in England: a whole-population study. The Lancet Diabetes & Endocrinology *S2213-8587*, 30272-30272.

Blume, C., Jackson, C.L., Spalluto, C.M., Legebeke, J., Nazlamova, L., Conforti, F., Perotin-Collard, J.-M., Frank, M., Crispin, M., Coles, J., et al. (2020). A novel isoform of ACE2 is expressed in human nasal and bronchial respiratory epithelia and is upregulated in response to RNA respiratory virus infection. bioRxiv.

Butler, A., Hoffman, P., Smibert, P., Papalexi, E., and Satija, R. (2018). Integrating single-cell transcriptomic data across different conditions, technologies, and species. Nat Biotechnol *36*, 411-420.

Campbell-Thompson, M., Wasserfall, C., Kaddis, J., Albanese-O'Neill, A., Staeva, T., Nierras, C., Moraski, J., Rowe, P., Gianani, R., Eisenbarth, G., et al. (2012). Network for Pancreatic Organ Donors with Diabetes (nPOD): developing a tissue biobank for type 1 diabetes. Diabetes Metab Res Rev.

Chen, L., and Hao, G. (2020). The Role of Angiotensin-Converting Enzyme 2 in Coronaviruses/Influenza Viruses and Cardiovascular Disease. Cardiovascular research, cvaa093.

Coate, K.C., Cha, J., Shrestha, S., Wang, W., Fasolino, M., Morgan, A., Dai, C., Saunders, D.C., Aramandla, R., Jenkins, R., et al. (2020). SARS-CoV-2 Cell Entry Factors ACE2 and TMPRSS2 are Expressed in the Pancreas but Not in Islet Endocrine Cells. bioRxiv.

Connors, J., and Levy, J. (2020). COVID-19 and its implications for thrombosis and anticoagulation. Blood *135*, 2033-2040.

DiMeglio, L.A., Albanese-O'Neill, A., Munoz, C.E., and Maahs, D.M. (2020). COVID-19 and Children With Diabetes-Updates, Unknowns, and Next Steps: First, Do No Extrapolation. Diabetes Care.

Dorward, D., Russell, C., Um, I., Elshani, M., Armstrong, S., Penrice-Randal, R., Millar, T., Lerpiniere, C., Tagliavini, G., Hartley, C., et al. (2020). Tissue-specific tolerance in fatal Covid-19. medRxiv.

Fignani, D., Licata, G., Brusco, N., Nigi, L., Grieco, G.E., Marselli, L., Overbergh, L., Gysemans, C., Colli, M.L., Marchetti, P., et al. (2020). SARS-CoV-2 receptor Angiotensin I-Converting Enzyme type 2 (ACE2) is expressed in human pancreatic β-cells and in the human pancreas microvasculature. bioRxiv.

Fox, S., Akmatbekov, A., Harbert, J., Li, G., Quincy Brown, J., and Vander Heide, R. (2020). Pulmonary and cardiac pathology in African American patients with COVID-19: an autopsy series from New Orleans. The Lancet. Respiratory medicine *8*, 681-686.

Goldman, N., Fink, D., Cai, J., Lee, Y., and Davies, Z. (2020). High Prevalence of COVID-19-associated Diabetic Ketoacidosis in UK Secondary Care. Diabetes research and clinical practice, 108291.

Grün, D., Muraro, M., Boisset, J., Wiebrands, K., Lyubimova, A., Dharmadhikari, G., van den Born, M., van, E.J., Jansen, E., Clevers, H., et al. (2016). De Novo Prediction of Stem Cell Identity using Single-Cell Transcriptome Data. Cell stem cell *19*, 266-277.

Hanley, B., Lucas, S., Youd, E., Swift, B., and Osborn, M. (2020). Autopsy in suspected COVID-19 cases. Journal of clinical pathology *73*, 239-242.

Hikmet, F., Méar, L., Edvinsson, Å., Micke, P., Uhlén, M., and Lindskog, C. (2020). The protein expression profile of ACE2 in human tissues. Molecular systems biology *16*, e9610.

Holman, N., Knighton, P., Kar, P., O'Keefe, J., Curley, M., Weaver, A., Barron, E., Bakhai, C., Khunti, K., Wareham, N., et al. (2020). Risk factors for COVID-19-related mortality in people with type 1 and type 2 diabetes in England: a population-based cohort study. The Lancet Diabetes & Endocrinology *S2213-8587*, 30271-30270.

Hussain, A., Mahawar, K., Xia, Z., Yang, W., and El-Hasani, S. (2020). Obesity and mortality of COVID-19. Meta-analysis. Obesity research & clinical practice *14*, 295-300.

Hönzke, K., Obermayer, B., Mache, C., Fatykhova, D., Kessler, M., Dökel, S., Wyler, E., Hoffmann, K., Schulze, J., Mieth, M., et al. (2020). Human Lungs Show Limited Permissiveness for SARS-CoV-2 Due to Scarce ACE2 Levels But Strong Virus-Induced Immune Activation in Alveolar Macrophages. Cell Press Sneak Peek.

Lawlor, N., George, J., Bolisetty, M., Kursawe, R., Sun, L., Sivakamasundari, V., Kycia, I., Robson, P., and Stitzel, M. (2017). Single-cell transcriptomes identify human islet cell signatures and reveal cell-type-specific expression changes in type 2 diabetes. Genome Research *27*, 208-222.

Lee, I.T., Nakayama, T., Wu, C.T., Goltsev, Y., Jiang, S., Gall, P.A., Liao, C.K., Shih, L.C., Schürch, C.M., McIlwain, D.R., et al. (2020a). Robust ACE2 protein expression localizes to the motile cilia of the respiratory tract epithelia and is not increased by ACE inhibitors or angiotensin receptor blockers. medRxiv *Preprint*.

Lee, J., Kopetz, S., Vilar, E., Shen, J., Chen, K., and Maitra, A. (2020b). Relative Abundance of SARS-CoV-2 Entry Genes in the Enterocytes of the Lower Gastrointestinal Tract. Genes *11*, 645.

Li, J., Wang, X., Chen, J., Zuo, X., Zhang, H., and Deng, A. (2020). COVID-19 infection may cause ketosis and ketoacidosis. Diabetes, obesity & metabolism, 1-7.

Liu, Q., Wang, R., Qu, G., Wang, Y., Liu, P., Zhu, Y., Fei, G., Ren, L., Zhou, Y., and Liu, L. (2020). Gross examination report of a COVID-19 death autopsy. Fa yi xue za zhi *36*, 21-23.

Marchand, L., Pecquet, M., and Luyton, C. (2020). Type 1 diabetes onset triggered by COVID-19. Acta diabetologica, 1-2.

Menter, T., Haslbauer, J., Nienhold, R., Savic, S., Hopfer, H., Deigendesch, N., Frank, S., Turek, D., Willi, N., Pargger, H., et al. (2020). Postmortem examination of COVID-19 patients reveals diffuse alveolar damage with severe capillary congestion and variegated findings in lungs and other organs suggesting vascular dysfunction. Histopathology *77*, 198-209.

Mercatelli, D., and Giorgi, F. (2020). Geographic and Genomic Distribution of SARS-CoV-2 Mutations. Frontiers in Microbiology *11*, 1800.

Muraro, M., Dharmadhikari, G., Grün, D., Groen, N., Dielen, T., Jansen, E., van Gurp, L., Engelse, M., Carlotti, F., de Koning, E., et al. (2016). A Single-Cell Transcriptome Atlas of the Human Pancreas. Cell systems *3*, 385-394.e383.

Nakeshbandi, M., Maini, R., Daniel, P., Rosengarten, S., Parmar, P., Wilson, C., Kim, J., Oommen, A., Mecklenburg, M., Salvani, J., et al. (2020). The impact of obesity on COVID-19 complications: a retrospective cohort study. International journal of obesity (2005) *44*, 1832-1837.

Ng, K., Attig, J., Bolland, W., Young, G.R., Major, J., Wack, A., and Kassiotis, G. (2020). Tissue-specific and interferon-inducible expression of non-functional ACE2 through endogenous retrovirus co-option. bioRxiv.

Onabajo, O., Banday, A., Stanifer, M., Yan, W., Obajemu, A., Santer, D., Florez-Vargas, O., Piontkivska, H., Vargas, J., Ring, T., et al. (2020). Interferons and viruses induce a novel truncated ACE2 isoform and not the full-length SARS-CoV-2 receptor. Nature genetics.

Rapkiewicz, A., Mai, X., Carsons, S., Pittaluga, S., Kleiner, D., Berger, J., Thomas, S., Adler, N., Charytan, D., Gasmi, B., et al. (2020). Megakaryocytes and platelet-fibrin thrombi characterize multi-organ thrombosis at autopsy in COVID-19: A case series. EClinicalMedicine *24*, 100434.

Segerstolpe, Å., Palasantza, A., Eliasson, P., Andersson, E., Andréasson, A., Sun, X., Picelli, S., Sabirsh, A., Clausen, M., Bjursell, M., et al. (2016). Single-Cell Transcriptome Profiling of Human Pancreatic Islets in Health and Type 2 Diabetes. Cell Metabolism *24*, 593-607.

Taneera, J., El-Huneidi, W., Hamad, M., Mohammed, A., Elaraby, E., and Hachim, M. (2020). Expression Profile of SARS-CoV-2 Host Receptors in Human Pancreatic Islets Revealed Upregulation of ACE2 in Diabetic Donors. Biology *9*, 215.

Tartof, S., Qian, L., Hong, V., Wei, R., Nadjafi, R., Fischer, H., Li, Z., Shaw, S., Caparosa, S., Nau, C., et al. (2020). Obesity and Mortality Among Patients Diagnosed With COVID-19: Results From an Integrated Health Care Organization. Annals of internal medicine, M20-3742.

The Lancet Diabetes Endocrinology (2020). COVID-19 and diabetes: a co-conspiracy? The Lancet Diabetes & Endocrinology *8*, 801.

Tipnis, S., Hooper, N., Hyde, R., Karran, E., Christie, G., and Turner, A. (2000). A human homolog of angiotensin-converting enzyme. Cloning and functional expression as a captopril-insensitive carboxypeptidase. The Journal of Biological Chemistry *275*, 33238-33243.

Tittel, S., Rosenbauer, J., Kamrath, C., Ziegler, J., Reschke, F., Hammersen, J., Mönkemöller, K., Pappa, A., Kapellen, T., Holl, R., et al. (2020). Did the COVID-19 Lockdown Affect the Incidence of Pediatric Type 1 Diabetes in Germany? Diabetes care, dc201633.

Unsworth, R., Wallace, S., Oliver, N.S., Yeung, S., Kshirsagar, A., Naidu, H., Kwong, R.M.W., Kumar, P., and Logan, K.M. (2020). New-Onset Type 1 Diabetes in Children During COVID-19: Multicenter Regional Findings in the U.K. Diabetes Care, dc201551.

Varga, Z., Flammer, A., Steiger, P., Haberecker, M., Andermatt, R., Zinkernagel, A., Mehra, M., Schuepbach, R., Ruschitzka, F., and Moch, H. (2020). Endothelial cell infection and endotheliitis in COVID-19. Lancet (London, England) *395*, 1417-1418.

Wang, F., Wang, H., Fan, J., Zhang, Y., Wang, H., and Zhao, Q. (2020). Pancreatic Injury Patterns in Patients With Coronavirus Disease 19 Pneumonia. Gastroenterology *159*, 367-370.

Wasserfall, C., Montgomery, E., Yu, L., Michels, A., Gianani, R., Pugliese, A., Nierras, C., Kaddis, J.S., Schatz, D.A., Bonifacio, E., et al. (2016). Validation of a rapid type 1 diabetes autoantibody screening assay for community-based screening of organ donors to identify subjects at increased risk for the disease. Clin Exp Immunol *185*, 33-41.

Wichmann, D., Sperhake, J., Lütgehetmann, M., Steurer, S., Edler, C., Heinemann, A., Heinrich, F., Mushumba, H., Kniep, I., Schröder, A., et al. (2020). Autopsy Findings and Venous Thromboembolism in Patients With COVID-19. Annals of internal medicine, M20-2003.

Yang, J., Lin, S., Ji, X., and Guo, L. (2010). Binding of SARS coronavirus to its receptor damages islets and causes acute diabetes. Acta diabetologica *47*, 193-199.

Yang, L., Han, Y., Nilsson-Payant, B., Gupta, V., Wang, P., Duan, X., Tang, X., Zhu, J., Zhao, Z., Jaffré, F., et al. (2020). A Human Pluripotent Stem Cell-based Platform to Study SARS-CoV-2 Tropism and Model Virus Infection in Human Cells and Organoids. Cell stem cell *27*, 125-136.

Zang, R., Gomez Castro, M., McCune, B., Zeng, Q., Rothlauf, P., Sonnek, N., Liu, Z., Brulois, K., Wang, X., Greenberg, H., et al. (2020). TMPRSS2 and TMPRSS4 promote SARS-CoV-2 infection of human small intestinal enterocytes. Science immunology *5*, eabc3582.

Zhou, F., Yu, T., Du, R., Fan, G., Liu, Y., Liu, Z., Xiang, J., Wang, Y., Song, B., Gu, X., et al. (2020). Clinical course and risk factors for mortality of adult inpatients with COVID-19 in Wuhan, China: a retrospective cohort study. Lancet *395*, 1054-1062.

Figure 1

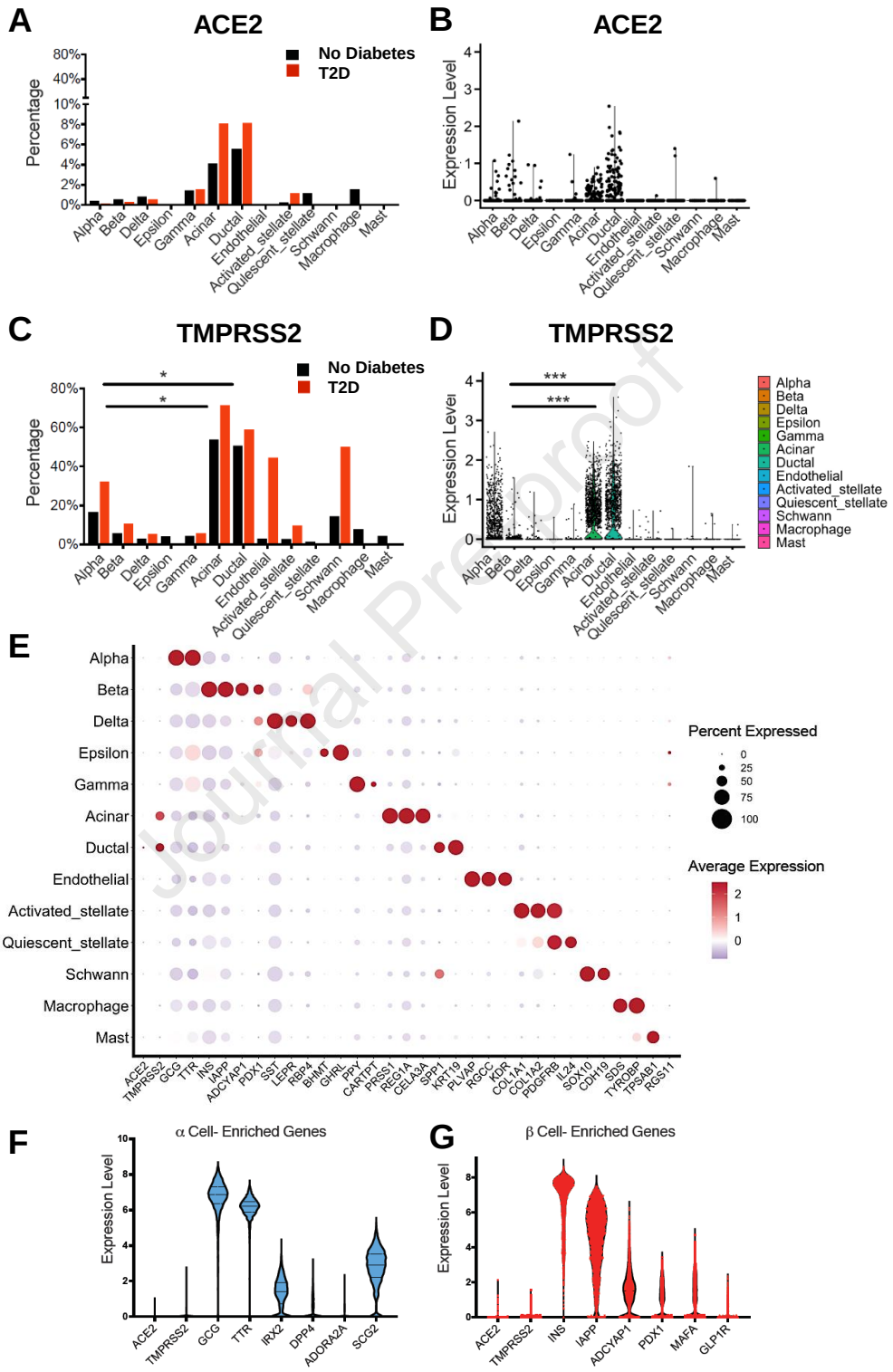

Figure 2

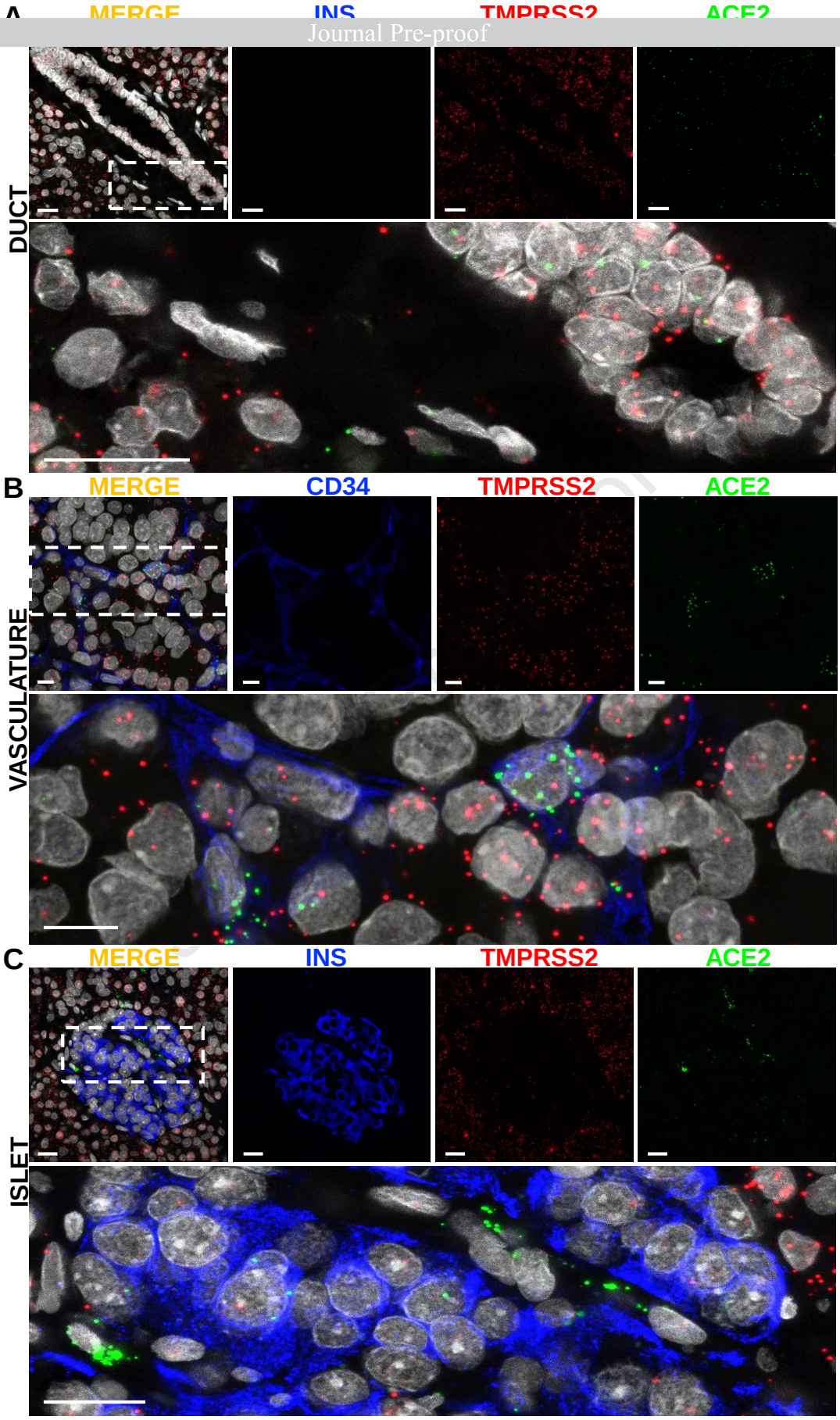

Figure 3

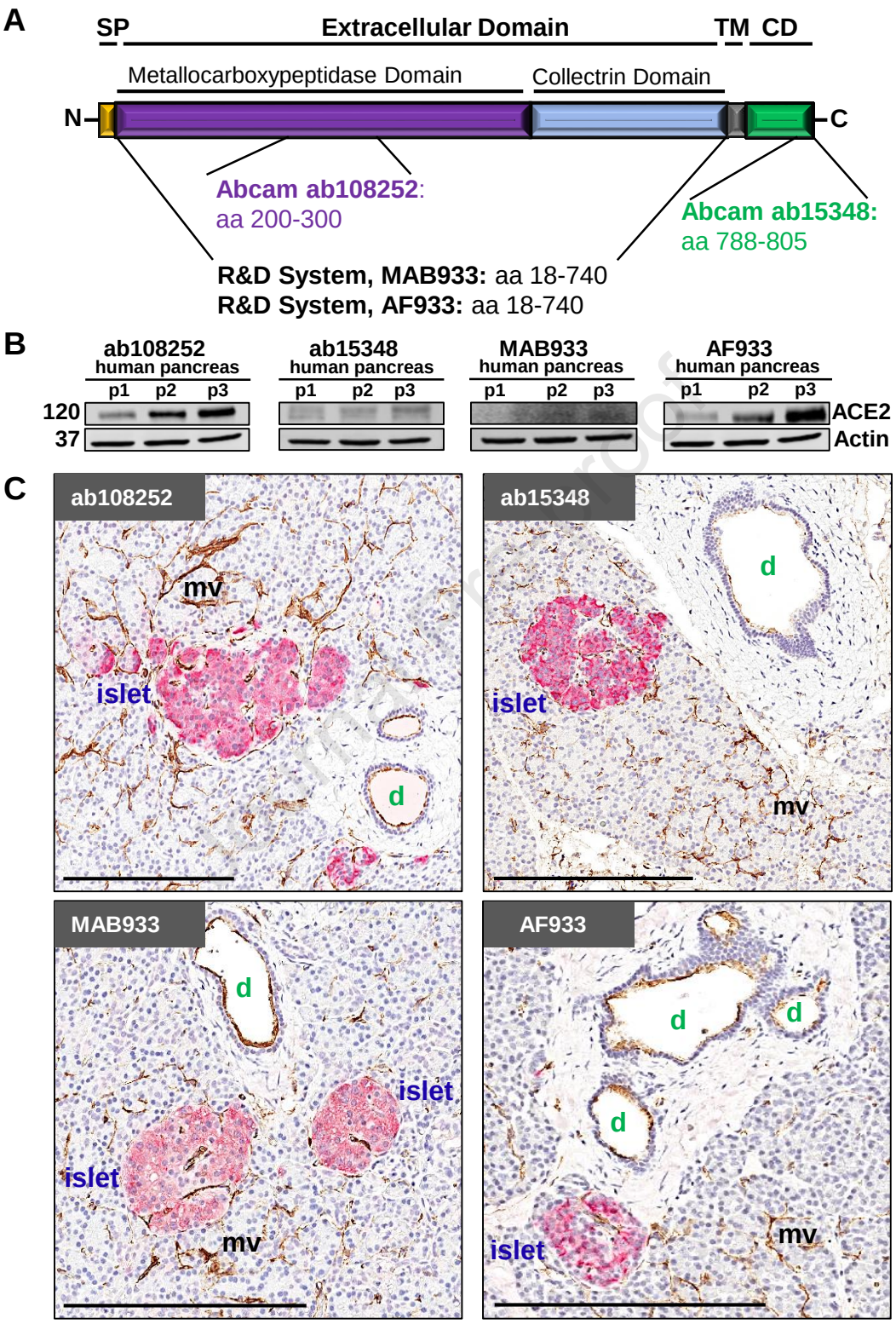
A
SP
Extracellular Domain
TM
CD
Metallocarboxypeptidase Domain
Collectrin Domain
N
C
Abcam ab108252:
aa 200-300
Abcam ab15348:
aa 788-805
R&D System, MAB933: aa 18-740
R&D System, AF933: aa 18-740
B
ab108252
human pancreas
ab15348
human pancreas
MAB933
human pancreas
AF933
human pancreas
p1 p2 p3
120
37
ACE2
Actin
C
ab108252
mv
islet
d
ab15348
d
islet
mv
MAB933
d
islet
islet
mv
AF933
d
d
d
islet
mv

Figure 3

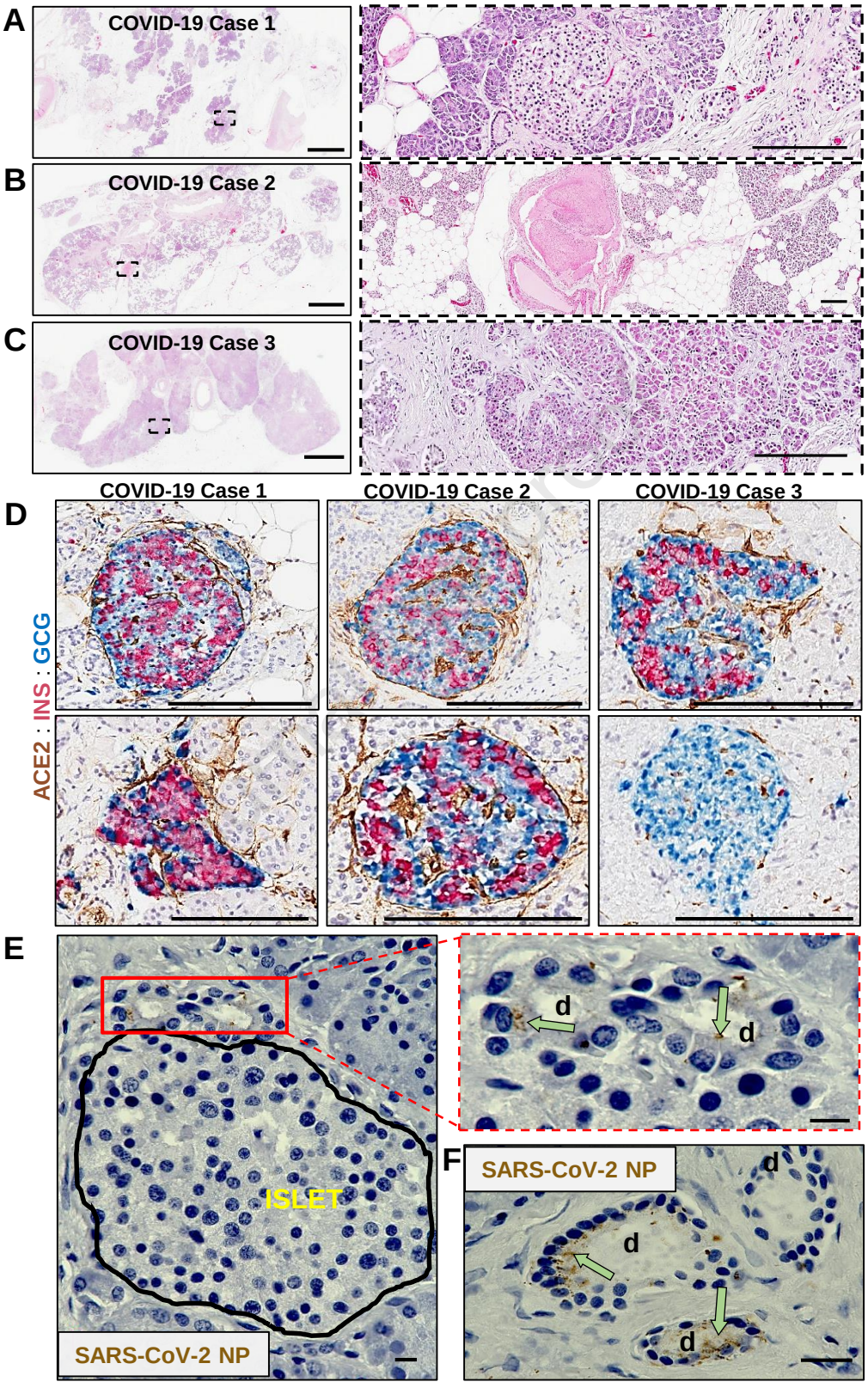
A
COVID-19 Case 1
B
COVID-19 Case 2
C
COVID-19 Case 3
D
COVID-19 Case 1
COVID-19 Case 2
COVID-19 Case 3
ACE2 : INS : GCG
E
ISLET
SARS-CoV-2 NP
d
d
F
SARS-CoV-2 NP
d
d
d

Figure 4

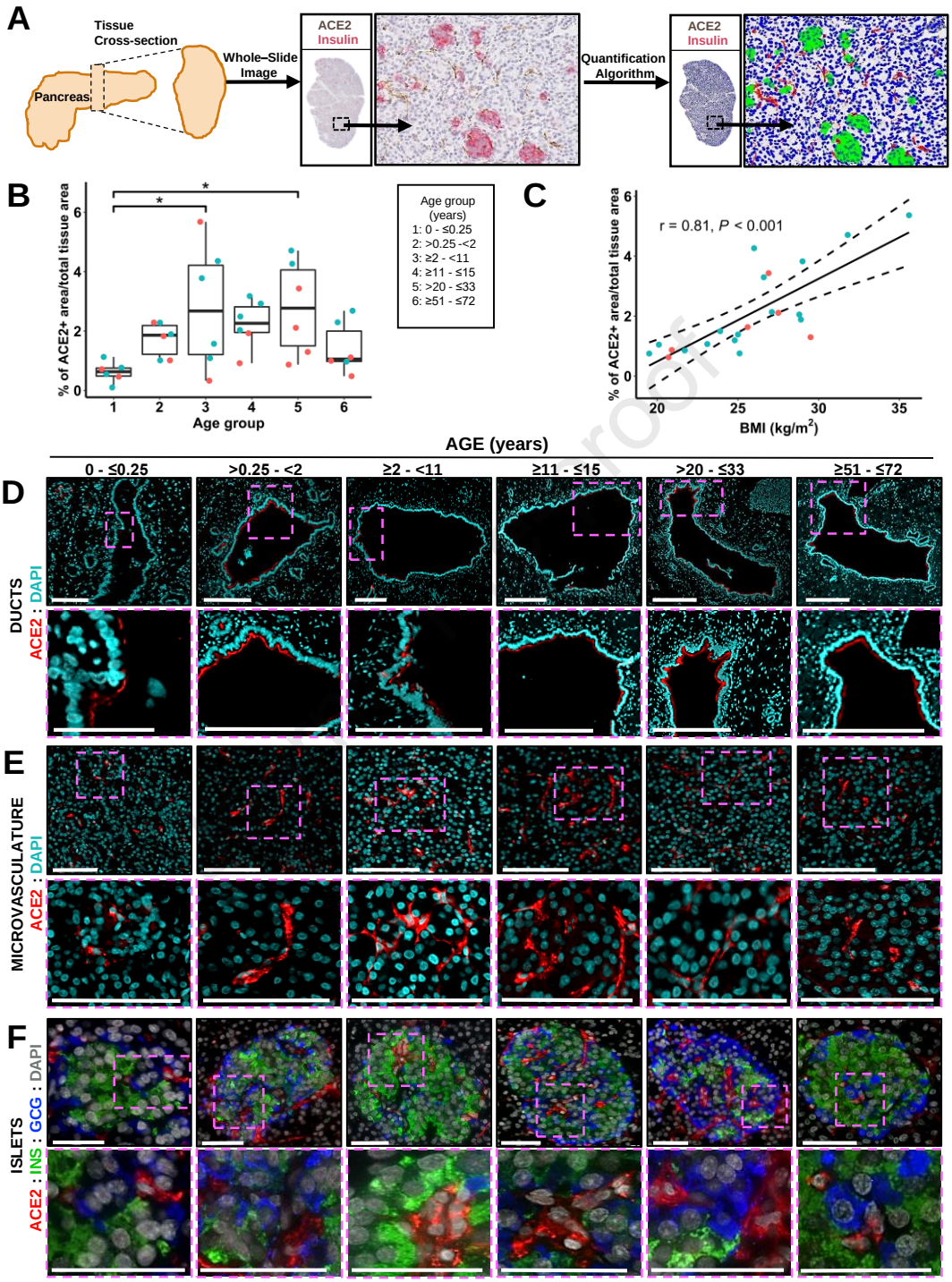
A
Tissue
Cross-section
Pancreas
Whole–Slide
Image
ACE2
Insulin
Quantification
Algorithm
B
% of ACE2+ area/total tissue area
Age group
Age group
(years)
1: 0 - ≤0.25
2: >0.25 -<2
3: ≥2 - <11
4: ≥11 - ≤15
5: >20 - ≤33
6: ≥51 - ≤72
C
r = 0.81, P < 0.001
% of ACE2+ area/total tissue area
BMI (kg/m²)
AGE (years)
0 - ≤0.25
>0.25 - <2
≥2 - <11
≥11 - ≤15
>20 - ≤33
≥51 - ≤72
D
DUCTS
ACE2 : DAPI
E
MICROVASCULATURE
ACE2 : DAPI
F
ISLETS
ACE2 : INS : GCG : DAPI

Highlights

- ACE2 mRNA and protein are expressed in human pancreatic ducts and microvasculature
- *ACE2* mRNA was rarely detected and at low levels in human pancreatic endocrine cells
- Pancreatic ACE2 protein expression changes across the lifespan and correlates with BMI
- SARS-CoV-2 NP was detected in ducts but not endocrine cells of COVID-19 pancreata

eTOC

Kusmartseva et al. demonstrate preferential ACE2 expression in pancreatic microvascular and ductal structures, suggesting these constitute a more likely target than islet endocrine cells in SARS-CoV-2 infection. This notion was supported by detection of SARS-CoV-2 nucleocapsid protein in ductal epithelium but not endocrine cells of pancreata from individuals with COVID-19.

KEY RESOURCES TABLE

REAGENT or RESOURCE	SOURCE	IDENTIFIER
Antibodies		
Rabbit monoclonal IgG anti-ACE2 (clone EPR4435(2))	Abcam	Cat# ab108252; RRID: AB_10864415
Rabbit polyclonal anti-ACE2	Abcam	Cat# ab15348; RRID: AB_301861
Mouse monoclonal IgG2A anti-human ACE2 (clone 171606)	R&D Systems	Cat# MAB933; RRID: AB_2223153
Goat polyclonal anti-human ACE2	R&D Systems	Cat# AF933; AB_355722
Biotinylated goat anti-rabbit IgG	Vector Laboratories	Cat# BA-1000: RRID: AB_2313606
Biotinylated horse anti-mouse IgG (H+L)	Vector Laboratories	Cat# BA-2000; RRID: AB_2313581
Biotinylated rabbit anti-goat IgG (H+L)	Vector Laboratories	Cat# BA-5000; RRID: AB_2336126
Mouse monoclonal IgG1κ anti-CD34 (clone QBEnd/10)	Novus Biologicals	Cat# NBP2-32932; RRID: AB_2861355
Rabbit monoclonal IgG anti-insulin (clone EPR17359)	Abcam	Cat# ab181547; RRID: AB_2716761
FLEX guinea pig polyclonal anti-insulin, ready-to-use antibody	Agilent	Cat# IR002; RRID: AB_2800361
Mouse monoclonal IgG1k anti-cytokeratin 19 (clone RCK108)	Agilent	Cat# M0888; RRID:AB_2234418
Goat anti-rabbit IgG (H+L), Alexa Fluor 594	Invitrogen	Cat# A-11037; RRID: AB_2534095
Goat anti-mouse IgG (H+L), Alexa Fluor 488	Invitrogen	Cat# A-11029; RRID: AB_2534088
Goat anti-rabbit IgG (H+L), Alexa Fluor 555	Invitrogen	Cat# A-21428; RRID: AB_2535849
Goat anti-guinea pig IgG (H+L), Alexa Fluor 647	Invitrogen	Cat# A21450; RRID: AB_2735091
Mouse monoclonal IgG1 anti-SARS/SARS-CoV-2 Coronavirus Nucleocapsid protein (clone B46F)	Invitrogen	Cat# MA-1-7404; RRID: AB_1018422
Mouse monoclonal IgG1 anti-glucagon (clone K79bB10)	Abcam	Cat# Ab10988; RRID: AB_297642
Mouse monoclonal IgG1 anti-β-actin (AC-15)	Sigma-Aldrich	Cat# A1978; RRID: AB_476692
Goat anti-guinea pig IgG (H+L), Alexa Fluor 488	Invitrogen	Cat# A-11073; RRID: AB_2534117
Donkey anti-mouse IgG (H+L), Alexa Fluor 488	Invitrogen	Cat# A-21202; RRID: AB_141607
IRDye 800CW Goat anti-rabbit IgG	LI-COR Biosciences	Cat# 926-32211; RRID: AB_621843
IRDye 800CW Goat anti-mouse IgG	LI-COR Biosciences	Cat# 926-32210; RRID: AB_621842
IRDye 800CW Donkey anti-goat IgG	LI-COR Biosciences	Cat# 926-32214; RRID: AB_621846
IRDye 680LT Donkey anti-mouse IgG	LI-COR Biosciences	Cat# 926-68022; RRID: AB_10715072
Bacterial and Virus Strains		

Biological Samples		
Human control organ donor duodenum blocks	nPOD; https://www.jdrfnpod.org/	Table S3
Human control organ donor kidney blocks	nPOD; https://www.jdrfnpod.org/	Table S3
Human control organ donor pancreas blocks	nPOD; https://www.jdrfnpod.org/	Table S3
Human COVID-19 autopsy pancreas blocks	Department of Pathology, Louisiana State University; https://www.medschool.lsuhsc.edu/pathology/	Table S4
Chemicals, Peptides, and Recombinant Proteins		
ACE2 peptide	Abcam	Cat# ab198988
Antibody diluent reagent	Life Technologies	Cat# 003118
ImmpactDAB	Vector Laboratories	Cat# SK-4105
VECTASHIELD® Antifade Mounting Medium with DAPI	Vector Laboratories	Cat# H-1200
Borg Decloaker RTU	BioCare Medical	Cat# BD1000G1
Background Sniper	BioCare Medical	Cat# BS966L
Protease inhibitor cocktail	Thermo Fisher Scientific	Cat# 78430
Phosphatase inhibitor cocktail	Thermo Fisher Scientific	Cat# 78428
Intercept™ Blocking Buffer	LI-COR Biosciences	Cat# 927-60001
Intercept™ Antibody Diluent	LI-COR Biosciences	Cat# 927-65001
ProLong™ Gold Antifade Mountant	Thermo Fisher Scientific	Cat# P36934
Precision Plus Protein All Blue Prestained Protein Standard	Bio-Rad	Cat# 1610373
Critical Commercial Assays		
Avidin/Biotin blocking kit	Vector Laboratories	Cat# SP-2001
Elite standard detection kit	Vector Laboratories	Cat# PK-6100
MACH 2 Double Stain Kit 1 - Anti-Mouse AP/Anti-Rabbit HRP	BioCare Medical	Cat# MRCT523L
MACH 2 Double Stain Kit 2 - Anti-Mouse HRP/ Anti-Rabbit AP	BioCare Medical	Cat# MRCT525L
Betazoid DAB Chromogen Kit	BioCare Medical	Cat# BDB2004L
Warp Red Chromogen Kit	BioCare Medical	Cat# WR806
Ferangi Blue Chromogen Kit	BioCare Medical	Cat# FB813S
RNAscope Multiplex Fluorescent V2 Kit	Advanced Cell Diagnostics	Cat# 323100
TSA Plus Cyanine 3 Fluorescence Kit	Perkin Elmer	Cat# NEL744001KT
TSA Plus Cyanine 5 Fluorescence Kit	Perkin Elmer	Cat# NEL745001KT
Pierce™ BCA Assay kit	Thermo Fisher Scientific	Cat# 23227

4-20% gradient Mini-PROTEAN TGX™ Stain-Free gel	Bio-Rad	Cat# 456-8095
Deposited Data		
Raw scRNAseq data generated using inDrop	Gene Expression Omnibus Repository; (Baron et al., 2016)	Table S1; GEO: GSE84133
Raw scRNAseq data generated using Celseq	Gene Expression Omnibus Repository; (Grün et al., 2016)	Table S1; GEO: GSE81076
Raw scRNAseq data generated using Celseq2	Gene Expression Omnibus Repository; (Muraro et al., 2016)	Table S1; GEO: GSE85241
Raw scRNAseq data generated using Fluidigm C1	Gene Expression Omnibus Repository; (Lawlor et al., 2017)	Table S1; GEO: GSE86469
Raw scRNAseq data generated using SMART-Seq2	ArrayExpress; (Segerstolpe et al., 2016)	Table S1; E-MTAB-5061
Raw and analyzed histology data	This paper	https://aperioeslide.ahc.ufl.edu
Experimental Models: Cell Lines		
Experimental Models: Organisms/Strains		
Oligonucleotides		
RNAscope® Probe- Hs-ACE2	Advanced Cell Diagnostics	Cat# 848151
RNAscope® Probe- Hs-TMPRSS2-C2	Advanced Cell Diagnostics	Cat# 470341-C2
RNAscope® Probe- Hs-TMPRSS4-C2	Advanced Cell Diagnostics	Cat# 565301
RNAscope® Probe- Hs-TMPRSS11D-C2	Advanced Cell Diagnostics	Cat# 870841-C4
RNAscope® Probe- Hs-CTSL-C2	Advanced Cell Diagnostics	Cat# 858611
RNAscope® Probe- Hs-ADAM 17-C2	Advanced Cell Diagnostics	Cat# 468141
Recombinant DNA		
Software and Algorithms		
Open-source Single-cell R Toolkit, Seurat v.3	Satija Lab; (Butler et al., 2018)	http://satijalab.org/seurat/
HALO v3.0.311.262	Indica Labs	https://indicalab.com/halo/
Other		
Nitrocellulose membranes	LI-COR Biosciences	Cat# 926-31092

Supplemental Figure 1. Expression patterns of SARS-CoV-2 associated genes, Related to Figure 1.

(A-B) Violin plot showing *ACE2* and *TMPRSS2* normalized gene expression in β-cells from donors with (*n* = 694 cells) and without type 2 diabetes (*n* = 2,985 cells). *ACE2* and *TMPRSS2* expression were not significantly different between groups, Wilcoxon rank sum tests. ND: No Diabetes, T2D: Type 2 Diabetes

(C) Violin plot showing the distribution of *TMPRSS4* normalized expression in the pancreas of donors without diabetes (*n* = 12,185 cells).

(D) Bar graphs showing the percentage of pancreatic cells with detectable *TMPRSS4* in donors with (*n* = 2,705 cells) and without type 2 diabetes (*n* = 12,185 cells). T2D: Type 2 Diabetes.

(E-G) Violin plots showing the distribution of *TMPRSS11D*, *CTSL*, and *ADAM17* normalized expression in the pancreas of donors without diabetes (*n* = 12,185 cells).

(H) Violin plot showing *CTSL* normalized gene expression in β-cells from donors with (*n* = 694 cells) and without type 2 diabetes (*n* = 2,985 cells). *CTSL* expression was higher in beta cells from donors with type 2 diabetes, Wilcoxon rank sum tests, adjusted $P = 8.94 \times 10^{-32}$, $*** P < 0.001$. ND: No Diabetes, T2D: Type 2 Diabetes. Violin plot limits show maxima and minima, and the dots represent individual data points.

Supplemental Figure 1

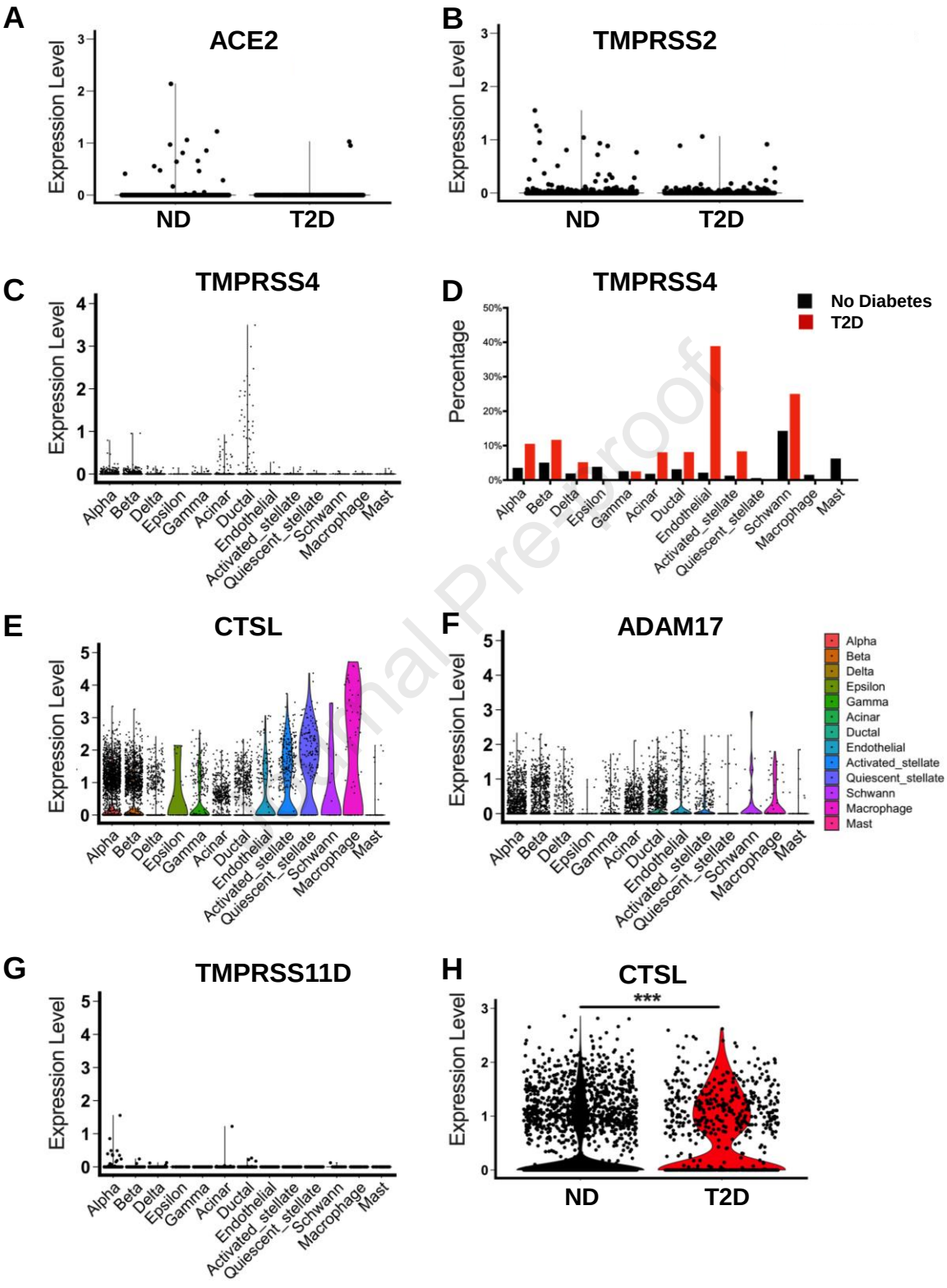

Supplemental Figure 2. Detection of SARS-CoV-2 associated gene expression in human pancreas using single molecular fluorescence *in situ* hybridization (smFISH), **Related to Figure 2 and STAR Methods.**

(A) Validation of smFISH probes in control human tissues. Single molecular fluorescent in-situ hybridization (smFISH) images of human duodenum, ileum, and kidney used as a positive controls to test the specificity of the probe sets used to determine the expression of *ACE2* and *TMPRSS2*.

(B) Validation of smFISH probes in control human tissues. smFISH images of human duodenum and kidney used as a positive controls to test the specificity of the probe sets used to determine the expression of *ACE2*, *TMPRSS4*, *TMPRSS11D*, *CTSL*, and *ADAM17*.

(C-F) Representative images of smFISH for **(C)** *ACE2* and *TMPRSS11D;* **(D)** *ACE2* and *CTSL;* **(E)** *ACE2* and *ADAM17;* **(F)** *ACE2* and *TMPRSS4;* mRNA in human pancreatic tissue sections counter stained for insulin. Inset highlights mRNA distribution in pancreatic islets; scale bar: 20μm.

Supplemental Figure 2

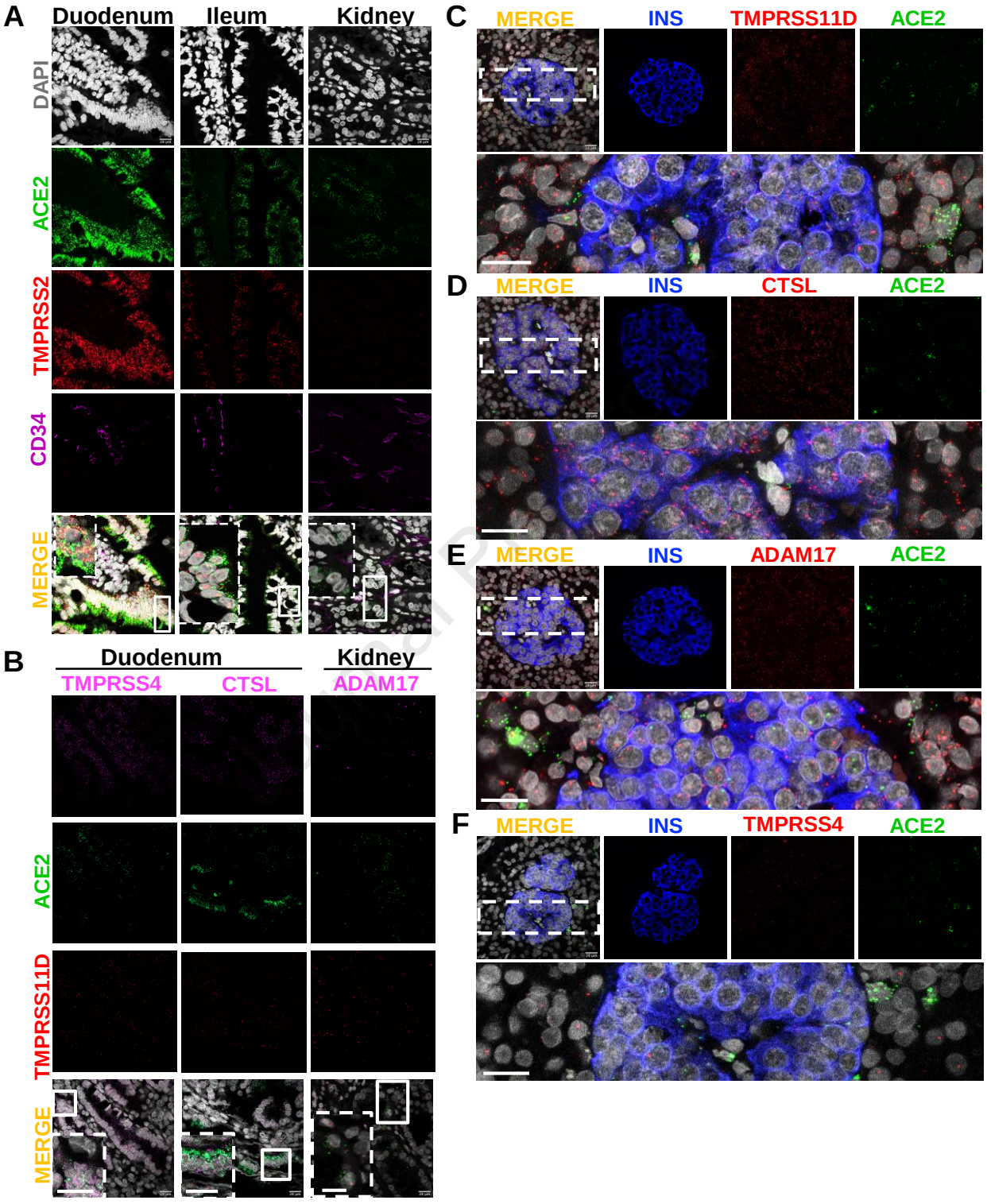

Supplemental Figure 3. Detection of ACE2 protein in human pancreatic tissue, Related to Figure 3 and STAR Methods.

(A) Detection ACE2 in protein lysate from three organ donors. Full immunoblot images of data presented in Figure 3A. Membranes were incubated with primary antibodies against ACE2 (as indicated on the figure), washed, and incubated with the corresponded secondary antibody. Protein bands were visualized using the Odyssey Li-Cor infrared imager. The molecular weight ladder (Bio-Rad, Cat.No. 1610373) was run in each gel to confirm the correct size of the ACE2 band.

(B) Total protein on the membrane for the corresponding blots shown above. Pancreas lysates were run in TGX stain-free gels (Bio-Rad). After electrophoresis, gels were activated under UV light for 5 minutes using a Gel Doc EZ imaging system (Bio-Rad) to label all tryptophan residues on proteins. Once photoactivated, proteins were transferred to nitrocellulose membranes. The stain-free signal from proteins on the membrane was imaged using the Gel Doc EZ system.

(C) Validation of ACE2 antibodies for immunohistochemistry. IHC images of human duodenum and kidney were used as positive controls to test the specificity of four commercially available ACE2 antibodies as indicated on the figure.

(D) ACE2 blocking peptide (Abcam, Cat# 198988) was used to confirm the specificity of Abcam rabbit monoclonal ACE2 antibody (Cat# ab108252). The image of pancreas tissue section stained for ACE2 showing absence of staining with the neutralized antibody. Scale bars: 300μm.

Supplemental Figure 3

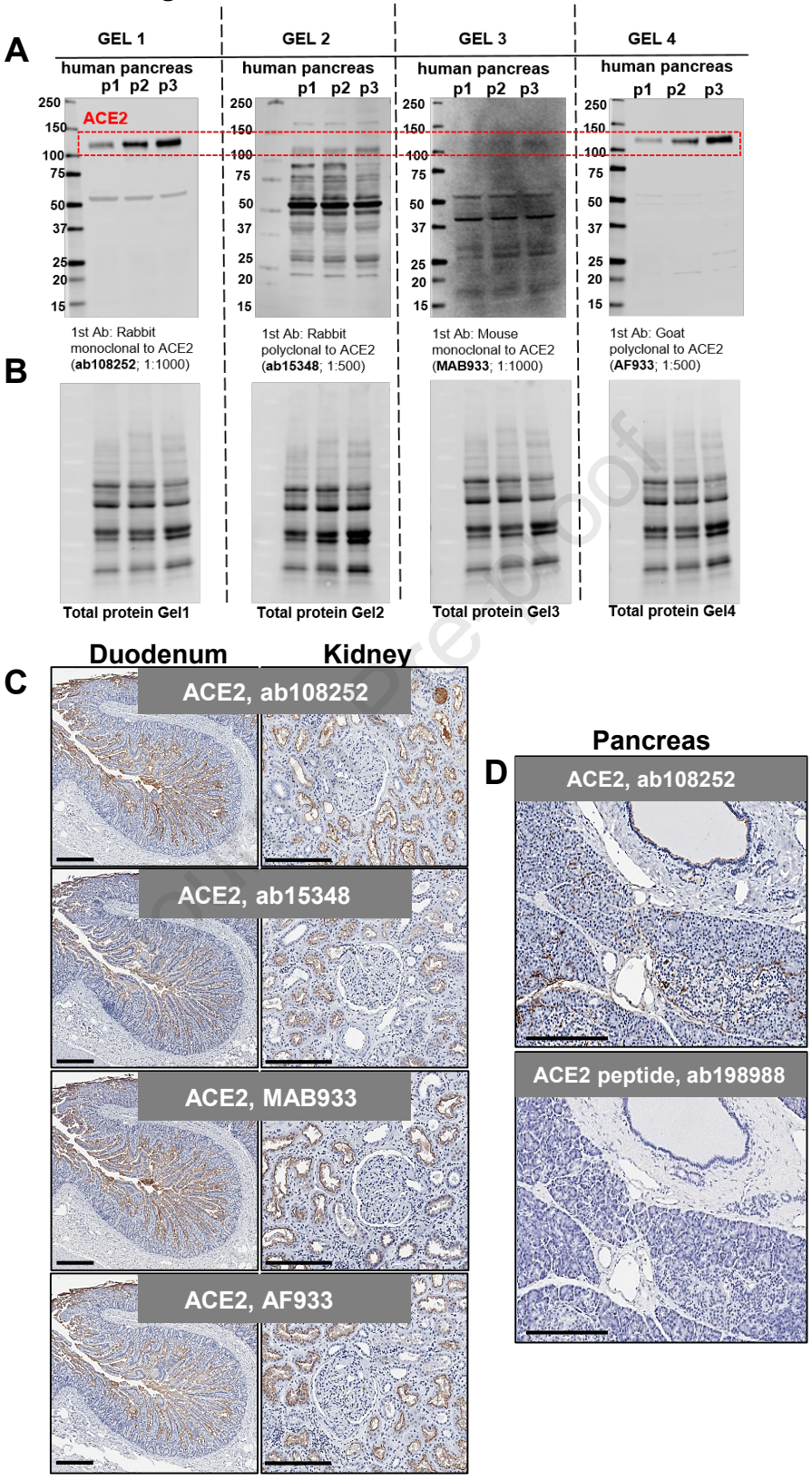

Supplemental Figure 4. ACE2 is highly expressed in microvasculature of the human pancreas, Related to Figure 3 and Figure 4.

(A) Representative image of pancreatic tissue section from SARS-CoV-2 negative donor without diabetes stained for ACE2 and Insulin. ACE2 positivity was associated with microvasculature in the acinar and islet regions Scale bars: 200μm.

(B) Representative immunofluorescence images showing lack of ACE2 protein expression in pancreatic blood vessels from control donors across different age groups. Scale bars (left to right): 100μm, 200μm, 200μm, 200μm, 200μm, 100μm.

(C) ACE2 expression by endothelial cells in the human pancreas. Representative immunofluorescence image of pancreatic tissue section stained for ACE2 (Abcam, ACE2 antibody Cat# ab108252) and endothelial cell marker CD34 (Novus Biological, mouse monoclonal CD34 antibody Cat# NBP2-32932).Endothelial cell positive for both ACE2 and CD34 markers are shown. Scale bars: 50μm.

Supplemental Figure 4

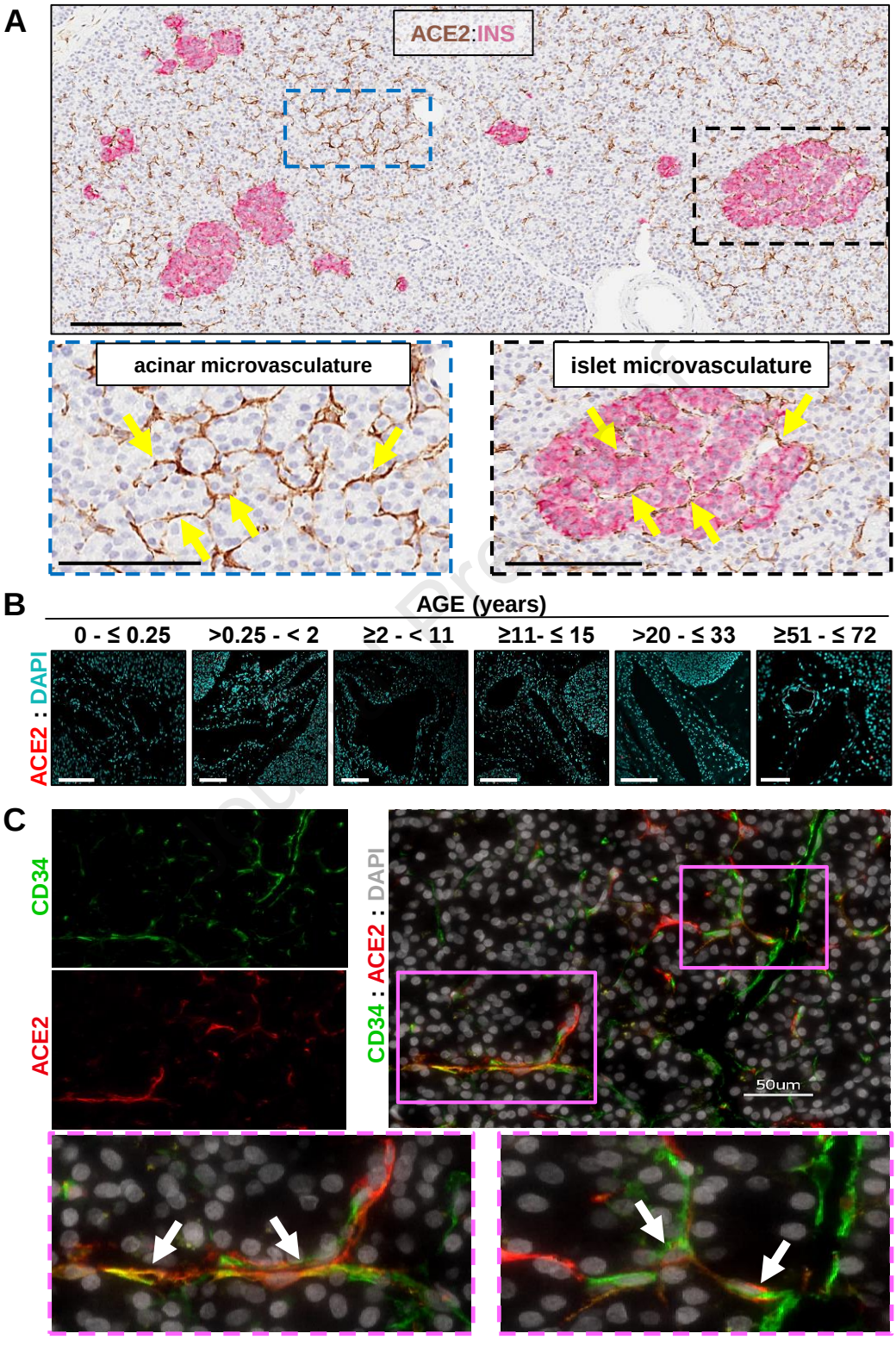

Supplemental Figure 5. Detection of SARS-CoV-2 nucleocapsid protein (NP) in the pancreas from individual with COVID-19, Related to Figure 5 and STAR Methods.

(A) Representative IHC image showing ACE2 protein expression in the pancreatic duct of COVID-19 Case 1. Scale bar: 200μm.

(B) IHC image of the human lung tissue sample known to be positive for SARS-CoV-2 used as positive control to test specificity of antibody against SARS-CoV-2 NP (clone B46F, Invitrogen, Cat# MA-1-7404). Scale bars: 50μm.

(C) Tissue section from pancreas of COVID-19 Case 1 showing the presence of SARS-CoV-2 NP in ductal epithelial cells. Scale bar: 200μm.

(D) Tissue section from pancreas of COVID-19 Case 1 stained with ductal cell marker cytokeratin 19 (CK 19) and SARS-CoV-2 NP. Scale bar: 200μm.

Supplemental Figure 3

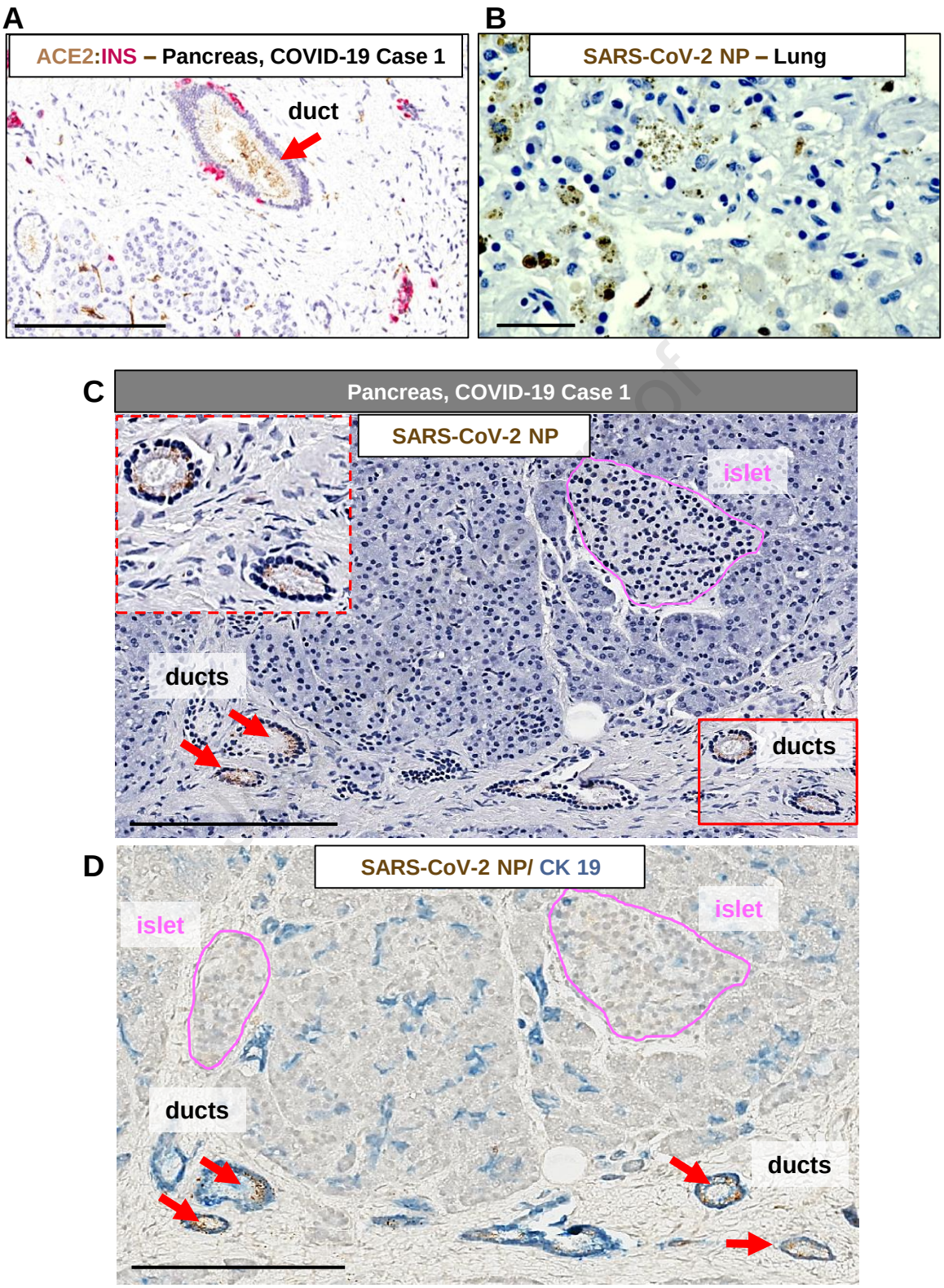

Supplemental Tables

Table S1. Gene expression by donor group and pancreatic cell type, Related to Figure 1A-D and Figure S1. From an integrated analysis of five public scRNAseq datasets (GSE84133 (Baron et al., 2016), GSE81076 (Grün et al., 2016), GSE85241 (Muraro et al., 2016), GSE86469 (Lawlor et al., 2017), and E-MTAB-5061 (Segerstolpe et al., 2016)), the number and percentage (presented as n (%)) of cells expressing *ACE2*, *TMPRSS2*, *TMPRSS4*, *CTSL*, *ADAM17*, *TMPRSS11D* are listed for each cell type from isolated islets from donors without diabetes (no diabetes; ND) or with type 2 diabetes (T2D).

Gene	Donor Group	Cell Type												
		Alpha	Beta	Delta	Epsilon	Gamma	Acinar	Ductal	Endothelial	Activated Stellate	Quiescent stellate	Schwann	Macrophage	Mast
ACE2	ND	15 (0.40)	17 (0.57)	7 (0.83)	0 (0.00)	6 (1.41)	70 (4.11)	81 (5.54)	0 (0.00)	1 (0.26)	2 (1.17)	0 (0.00)	1 (1.54)	0 (0.00)
	T2D	1 (0.12)	2 (0.29)	1 (0.57)	0 (0.00)	3 (1.52)	13 (8.07)	40 (8.13)	0 (0.00)	1 (1.19)	0 (0.00)	0 (0.00)	0 (0.00)	0 (0.00)
TMPRSS2	ND	624 (16.55)	163 (5.46)	24 (2.86)	1 (3.85)	18 (4.22)	915 (53.73)	739 (50.55)	8 (2.88)	10 (2.56)	2 (1.17)	3 (14.29)	5 (7.69)	2 (4.17)
	T2D	271 (32.07)	73 (10.52)	9 (5.17)	0 (0.00)	11 (5.56)	115 (71.43)	289 (58.74)	8 (44.44)	8 (9.52)	0 (0.00)	2 (50.00)	0 (0.00)	0 (0.00)
TMPRSS4	ND	134 (3.55)	151 (5.06)	16 (1.91)	1 (3.85)	11 (2.58)	31 (1.82)	46 (3.15)	6 (2.16)	5 (1.28)	1 (0.58)	3 (14.29)	1 (1.54)	3 (6.25)
	T2D	89 (10.53)	81 (11.67)	9 (5.17)	0 (0.00)	5 (2.53)	13 (8.07)	40 (8.13)	7 (38.89)	7 (8.33)	0 (0.00)	1 (25.00)	0 (0.00)	0 (0.00)
CTSL	ND	1375 (36.47)	1006 (33.70)	206 (24.55)	11 (42.31)	145 (33.96)	353 (20.73)	344 (23.53)	98 (35.25)	228 (58.46)	123 (71.93)	9 (42.86)	42 (64.62)	7 (14.58)
	T2D	617 (73.02)	409 (58.93)	97 (55.75)	3 (75.00)	147 (74.24)	91 (56.52)	318 (64.63)	9 (50.00%	70 (83.33)	7 (77.78)	3 (75.00)	13 (92.86)	2 (25.00)
ADAM17	ND	709 (18.81)	512 (17.15)	140 (16.69)	3 (11.54)	97 (22.72)	409 (24.02)	483 (33.04)	80 (28.78)	116 (29.74)	12 (7.02)	8 (38.10)	24 (36.92)	6 (12.50)
	T2D	370 (43.79)	214 (30.84)	61 (35.06)	2 (50.00)	97 (48.99)	90 (55.90)	316 (64.23)	12 (66.67)	39 (46.43)	3 (33.33)	2 (50.00)	6 (42.86)	3 (37.50)
TMPRSS11D	ND	17 (0.45)	2 (0.07)	3 (0.36)	0 (0.00)	0 (0.00)	4 (0.23)	5 (0.34)	0 (0.00)	0 (0.00)	0 (0.00)	1 (4.76)	0 (0.00)	0 (0.00)
	T2D	16 (1.89)	7 (1.01)	0 (0.00%	0 (0.00)	5 (2.53)	2 (1.24)	8 (1.63)	0 (0.00)	1 (1.19)	(0.00)	(0.00)	(0.00)	(0.00)

Table S2. ACE2 and viral entry protein co-expression patterns, Related to Figure 1. From an integrated analysis of five public scRNAseq datasets (GSE84133 (Baron et al., 2016), GSE81076 (Grün et al., 2016), GSE85241 (Muraro et al., 2016), GSE86469 (Lawlor et al., 2017), and E-MTAB-5061 (Segerstolpe et al., 2016)), the number and percentage (presented as n (%)) of cells co-expressing *ACE2* with *TMPRSS2*, *TMPRSS4*, *CTSL*, *ADAM17*, *TMPRSS11D* are listed for each cell type from isolated islets from donors without diabetes (no diabetes; ND) or with type 2 diabetes (T2D).

Gene Pairs	Donor Group	Cell Type												
		Alpha	Beta	Delta	Epsilon	Gamma	Acinar	Ductal	Endothelial	Activated Stellate	Quiescent stellate	Schwann	Macrophage	Mast
ACE2+/ TMPRSS2+	ND	9 (0.24)	3 (0.10)	2 (0.24)	0 (0.00)	0 (0.00)	65 (3.82)	63 (4.31)	0 (0.00)	0 (0.00)	0 (0.00)	0 (0.00)	1 (1.54)	0 (0.00)
	T2D	0 (0.00)	0 (0.00)	1 (0.57)	0 (0.00)	0 (0.00)	13 (8.07)	30 (6.10)	0 (0.00)	0 (0.00)	0 (0.00)	0 (0.00)	0 (0.00)	0 (0.00)
ACE2+/ TMPRSS4+	ND	3 (0.08)	2 (0.07)	2 (0.24)	0 (0.00)	0 (0.00)	4 (0.23)	5 (0.34)	0 (0.00)	0 (0.00)	0 (0.00)	0 (0.00)	0 (0.00)	0 (0.00)
	T2D	0 (0.00)	1 (0.14)	1 (0.57)	0 (0.00)	0 (0.00)	2 (1.24)	2 (0.41)	0 (0.00)	0 (0.00)	0 (0.00)	0 (0.00)	0 (0.00)	0 (0.00)
ACE2+/ CTSL+	ND	9 (0.24)	10 (0.34)	2 (0.24)	0 (0.00)	5 (1.17)	25 (1.47)	47 (3.21)	0 (0.00)	0 (0.00)	1 (0.58)	0 (0.00)	0 (0.00)	0 (0.00)
	T2D	1 (0.12)	2 (0.29)	1 (0.57)	0 (0.00)	3 (1.52)	11 (6.83)	40 (8.13)	0 (0.00)	1 (1.19)	0 (0.00)	0 (0.00)	0 (0.00)	0 (0.00)
ACE2+/ ADAM17+	ND	8 (0.21)	7 (0.23)	4 (0.48)	0 (0.00)	5 (1.17)	41 (2.41)	45 (3.08)	0 (0.00)	1 (0.26)	0 (0.00)	0 (0.00)	1 (1.54)	0 (0.00)
	T2D	1 (0.12)	2 (0.29)	0 (0.00)	0 (0.00)	3 (1.52)	12 (7.45)	37 (7.52)	0 (0.00)	0 (0.00)	0 (0.00)	0 (0.00)	0 (0.00)	0 (0.00)
ACE2+/ TMPRSS11D+	ND	0 (0.00)	0 (0.00)	1 (0.12)	0 (0.00)	0 (0.00)	0 (0.00)	0 (0.00)	0 (0.00)	0 (0.00)	0 (0.00)	0 (0.00)	0 (0.00)	0 (0.00)
	T2D	0 (0.00)	0 (0.00)	0 (0.00)	0 (0.00)	0 (0.00)	1 (0.62)	0 (0.00)	0 (0.00)	0 (0.00)	0 (0.00)	0 (0.00)	0 (0.00)	0 (0.00)

Table S3. Donor characteristics, Related to Figure 3, Figure 4, and STAR Methods. Tissues from 56 non-diabetic, SARS-CoV-2 negative donors were selected from the nPOD biobank and subjected to assays as detailed in the far-right column. Abbreviations: nPOD ID, Network for Pancreatic Organ donors with Diabetes Identification Number; yrs, years; BMI, body mass index; IHC, chromogen-based immunohistochemistry; IF, immunofluorescence; smFISH, single molecule fluorescence *in situ* hybridization.

*Some donors had hypertension in their anamnesis, but none of the donors evaluated received ACE inhibitors or angiotensin II receptor.

nPOD ID	Age (yrs)	Sex	Race/Ethnicity	BMI (kg/m^2)	Histopathology by nPOD	Technique Performed
6012*	68	Female	Caucasian	23.7	Ins+/Gluc+ normal islets, high density tail. Mild chronic pancreatitis, IPMN in PanHead (gastric type). Moderate exocrine fatty infiltrate.	IHC
6013	65	Male	Caucasian	24.2	Ins+/Gluc+ normal islets. Focal, moderate ductular metaplasia.	IHC, IF, smFISH
6017*	59	Female	Caucasian	24.8	Ins+/Gluc+ normal islets. Fatty infiltration-mild	IHC
6021*	72	Female	Hispanic	24.5	Ins+/Gluc+ normal islets. Extra-acinar islets. Low Ki67. Mucinous ductal dysplasia. Multi-focal mild acinar atrophy and fatty infiltration.	IHC, IF
6030	30.1	Male	Caucasian	27.1	Ins+/Gluc+ islets. Moderate Ki67 islets and other compartments. Sludge in ducts PanHead 05 and 10. Infrequent ductal islet units.	IHC
6057	22	Male	Caucasian	26	Ins+/Gluc+ normal islets, High Ki67+ most compartments	IHC
6091	27.1	Male	Caucasian	35.6	Ins+/Gluc+ normal islets, many large especially in head and body. Degree of fatty infiltrate moderate. No infiltrates identified.	IHC
6092	0.5	Female	African Am	13.8	Ins+ normal. High Ki67+ islets and acinar.	IHC
6106	2.9	Male	Caucasian	17.4	Ins+/Gluc+ normal islets. Low Ki67 acinar and islet but multifocal, mild duct proliferation.	IHC
6126	25.2	Male	Hispanic	25.1	Ins+/Gluc+ islets, normal. Moderate Ki67 acinar cells and occ. islets.	IHC
6125	0.42	Male	Caucasian	18.9	Ins+/Gluc+ normal islets. High acinar Ki67+.	IHC
6130	5.2	Male	Caucasian	18.5	Ins+ normal islets; low Ki67 in acinar and islets. No infiltrates.	IHC
6131	24.2	Male	Caucasian	24.8	Ins+/Gluc+ islets. Occ. high islet Ki67.	IHC
6134	26.7	Male	Caucasian	20.1	Ins+/Gluc+ islets plentiful, some with vascular stasis. Low Ki67.	IHC
6137	8.9	Female	Hispanic	24.2	Ins+ islets. Occ. islet with 3 or more Ki67+ cell. Mild fatty infiltrate. No inflammatory infiltrates.	IHC
6162	22.7	Male	African Am	28.9	Ins+/Gluc+ islets, plentiful. Very mild, focal acinar atrophy.	IHC
6160	22.1	Male	Caucasian	23.9	Ins+/Gluc+ islets present, all sizes. No infiltrates. Low Ki67.	IHC
6164	0	Male	Caucasian	16.5	Ins+/Gluc+ islets, plentiful. Multifocal lymphoid (high CD3+) aggregates or early PLN. High Ki67 islets and acinar regions.	IHC
6168	51	Male	Hispanic	25.2	Ins+/Gluc+ islets, all sizes. Normal density. Low Ki67. Variable fatty infiltrates acinar regions.	IHC, IF
6174	20.9	Male	Caucasian	19.5	Ins+/Gluc+ islets, plentiful. Low Ki67. No infiltrates.	IHC
6178	24.5	Female	Caucasian	27.5	Ins+/Gluc+ normal islets. Low Ki67. No infiltrates.	IHC
6179	20	Female	Caucasian	20.7	Ins+/Gluc+ islets, normal range of sizes, morphologies and density. Very high acinar Ki67. No other significant abnormalities observed.	IHC

6187	0.4	Male	Caucasian	17.1	Ins+/Gluc+ normal islets, numerous. No inflammation. Low islet Ki67, moderate acinar Ki67.	IHC, IF
6218	0.08	Female	African Am	17.2	Ins+/Gluc+ islets, normal. No abnormalities observed.	IHC, IF
6222	0.17	Male	Caucasian	16.4	Ins+/Gluc+ islets, numerous. High exocrine Ki67 with focal high duct Ki67+. Islets with Ki67+ cells in occ. islets head and body with more in tail region	IHC
6229	31	Female	Caucasian	26.9	Ins+/Gluc+ islets, no abnormalities observed. Occasional islet hyperemia.	IHC
6232	14	Female	Caucasian	20.8	Ins+/Gluc+ islets, numerous. No significant findings. 0-4 Ki67+ cells per islet, some non-insulin, as expected for this age. Low acinar Ki67.	IHC
6234	20	Female	Caucasian	25.6	Ins+/Gluc+ islets. No abnormalities observed. Low Ki67 all compartments.	IHC
6238	20	Male	African Am	21.7	Ins+/Gluc+ islets, normal numbers. Low Ki67. No major infiltrates. Focal hemorrhage and compression of acinar tissue.	IHC
6251	33	Female	Caucasian	29.5	Ins+/Gluc+ islets, numerous, including single cells. Infrequent islet with 1-3 Ki67+ cells. No significant lesions.	IHC, IF, Western Blot
6282	14	Male	Caucasian	41.9	Ins+/Gluc+ islets, numerous, small to large islet size range. High islet Ki67+ (2-5+ cells/islet).	IHC, IF
6290	58	Male	Caucasian	22.5	Ins+/Gluc+ islets, numerous. Multifocal extra- and intracinar regions with moderate fat content. Very mild chronic pancreatitis, focal (PanTail).	IHC
6313	0.25	Male	Caucasian	15.5	Ins+/Gluc islets, mostly small, numerous islets. Moderate acinar and islet Ki67+. No CD3 infiltrates observed.	IHC, IF, smFISH
6315	1.6	Male	African Am	14.7	Ins+/Gluc+ islets, normal sizes and morphologies. Moderate acinar Ki67+ while islets have low Ki67+. No infiltrates or other significant lesions.	IHC
6339	23.3	Male	Caucasian	25	Ins+/Gluc+ islets, normal morphologies and sizes including rare islets with reduced ratio beta to alpha cells. Very mild sporadic CD3+ periductal infiltrates. Mild to moderate interlobular fat. Mild increase acinar Ki67.	IHC
6348	0.03	Female	African Am	11.9	Ins+/Gluc+ islets, clusters, single cells. Well formed acini and lobules throughout. Very high Ki67 acini and islets.	IHC
6353	13	Male	African Am	28.3	Ins+/Gluc+ islets, range of normal sizes with rare islet >500um. Moderate islet Ki67+. Mild extra-pancreatic fat. Low acinar Ki67+ and CD3+ cell numbers.	IHC, IF
6356	1.58	Female	Caucasian	17.1	Ins+/Gluc+ islets, normal range of sizes and morphologies. Very mild focal islet hyperplasia ventral lobe. Acinar Ki67+ cell numbers mild with very Ki67+ islets for donor age.	IHC, IF, smFISH
6370	0	Male	Caucasian	11.4	Ins+/Gluc+ islets, expected numbers and morphologies including numerous single cells and clusters. High exocrine Ki67+ cell numbers but infrequent Ki67+ beta cells. Minimal exocrine CD3+ cell numbers.	IHC
6375	28.7	Male	Caucasian	31.8	Ins+/Gluc+ islets, normal numbers and sizes. Highly variable islet Ki67+ numbers with some having very high Ki67+. Low acinar Ki67+. Low with focally increased intralobular fat. Low exocrine infiltrates.	IHC
6376	0.6	Female	Caucasian	19.4	Ins+/Gluc+ islets, expected range of small to medium sized islets with regular morphology. Moderate Ki67+ acinar cells with focally high numbers in tail region. Low islet Ki67+ cells. Tail region has multifocal, very mild CD3+ infiltrates.	IHC
6387	15.6	Male	Caucasian	18.1	Ins+/Gluc+ islets, density, sizes, and morphologies within normal range. Low Ki67 except for few islets with mild increases, often non-beta cell. Low (normal) exocrine infiltrates.	IHC
6406	6.9	Male	Caucasian	16.8	Ins+/Gluc+ islets within normal range of sizes, shapes and density per region.	IHC, IF, smFISH
6415	10.9	Male	African Am	14.8	Ins+/Gluc+ islets range of normal sizes, numbers and morphologies. Acinar and islet Ki67+ cell numbers low (0-2) to occasional low-moderate (3-10).	IHC
6453	23.44	Male	Hispanic	23.1	Ins+/Gluc+ islets, wide range sizes, including very small to clusters, large islets (>500um) with predominance of alpha-cells and diffuse spreading. Mild islet fibrosis. Mild variable fat infiltration lobules. Slight autolysis (<20%).	IHC
6461	14.29	Male	Caucasian	18.5	Ins+/Gluc+ islets, mostly small to medium with regular morphology. Rare possible Ins- islet and small islets or clusters of alpha cells. No significant lesions observed.	IF, smFISH

6467	13.83	Male	Caucasian	19.6	Ins+/Gluc+ islets expected range of sizes, morphologies and densities with single beta-cells widely scattered.	IHC
6474	21.12	Male	African Am	29	Ins+/Gluc+ islets, numerous medium to large (400-500 um) with widely scattered alpha cells in periphery of several islets. Scattered foci GCG+ cells acinar regions. Mild increase islet Ki67+ cell numbers (2-5/islet). Widely scattered, mild increase in CD3+ cells within acinar regions. Various other examples of normal endocrine populations including ductal islet units of all endocrine populations and single and clustered PP+ cells in PanTail blocks.	IHC
6479	21.67	Female	Hispanic	20.9	Ins+/Gluc+ islets, normal range of sizes, morphologies and densities. Mild (head, body) to moderate lobular fatty infiltration.	IHC
6488	4.6	Female	Caucasian	16.8	Ins+/Gluc+ islets, normal range of sizes, morphologies and densities. Abundant single beta- and alpha-cells. Mild increase exocrine Ki67+ cell numbers due to mild leukocytic infiltrate as often seen.	IHC
6492	28.56	Male	Hispanic	26.6	Ins+/Gluc+ islets, a wide range of sizes with mostly spherical morphologies including numerous single endocrine cells or clusters. Few islets with high Ki67 and CD3+ cell numbers.	IHC
6493	18.84	Male	Caucasian	17.7	Ins+/Gluc+ islets, normal sizes and morphologies including single endocrine cells in acinar regions. No significant lesions observed.	IHC, IF, Western Blot
6495	9.6	Male	Caucasian	10.7	Ins+/Gluc+ islets, normal range of sizes including some large (800um) with regular morphologies and densities per region. No significant lesions.	Western Blot
6500	14.14	Female	African Am	19.7	Ins+/Gluc+ islets, wide range of sizes and mostly spherical morphologies. No significant lesions.	IHC
6516	20.75	Male	Caucasian	28.8	Ins+/Gluc+ islets, normal range of sizes, numbers and shapes. No significant findings.	IF, smFISH
6518	21.86	Male	Caucasian	23.8	(Preliminary): islets plentiful, normal numbers, morphology.	IHC

Table S4. Demographic and clinical information for COVID-19 cases, Related to Figure 5 and Figure S5C-D. Pancreas was obtained at autopsy from three patients with fatal coronavirus disease 2019 (COVID-19). Abbreviations: yr, years; African Am, African American; BMI, body mass index; Type 2 DM, Type 2 diabetes; appx, approximately.

	COVID-19 Case 1	**COVID-19 Case 2**	**COVID-19 Case 3**
Age at Death (yr)	72	45	71
Sex	Male	Male	Male
Race	Caucasian	African Am	African Am
BMI (kg/m^2)	14.9	49.0	26.3
Diabetes Status	No diabetes	Type 2 DM	Type 2 DM
Diabetes Duration	----	unknown	unknown
Blood Glucose (mg/dL) at admission at death	 94 121	 156 238	 264 134
Reported Days Ill Prior to Hospital Admission	Unknown (appx 1 week nursing home)	2	4
Days from Admission to Death	51	8	39